To the Graduate Council:

I am submitting herewith a thesis written by Lenora Lorraine Jones entitled "Gas Phase Diagnostics for CVD Diamond Growth." I have examined the final copy of this thesis for form and content and recommend that it be accepted in partial fulfillment of the requirements for the degree of Master of Science, with a major in Chemistry.

Charles S. Feigerle, Ph.D.

We have read this thesis
and recommend its acceptance:

Accepted for the Council:

Associate Vice Chancellor and
Dean of The Graduate School

Gas Phase Diagnostics for CVD Diamond Growth

A Thesis
Presented for the
Master of Science Degree

The University of Tennessee, Knoxville

Lenora Lorraine Jones
December 1995

Dedication

This thesis is dedicated to my parents

David and Sherry Jones

and to my brother

Mathew Jones

for all the love, support (emotional and financial),
and encouragement
they have given me during this trying time.

Acknowledgments

I am grateful for the help and encouragement Chuck Feigerle has given me throughout my graduate studies. Without his initial invitation to work with him, I am almost certain I would have missed out on this interesting project and experience. I am also appreciative of the guidance provided by the other members of my committee: Fred Grimm and Earl Wehry.

I would like to thank Bob Shaw for his "hands on" guidance of my graduate research. His almost daily "science lessons" added so much to my education. I also extend my gratitude to the other members of the Laser Spectroscopy Group at Oak Ridge National Laboratory in Oak Ridge, TN. Each played varying roles in this accomplishment. My deepest gratitude to visiting Professors LinJun Wang (programming whiz) and Jing-yuan Zhang (laser whiz) for their knowledge and contributions to this project.

Thanks to Dr. Robert Clausing and Lee Heatherly for teaching me about diamond morphology. (I got to learn from the BEST!) A special thanks also to Dr. Anna Edwards for running all the Raman spectra presented in this thesis.

A special thanks to Kathy and Christy who kept me in graduate school. I know at times they wondered if I would return to UT after a vacation. (At the time, it was a very difficult act, but now it's finally done!) Thanks for being

great friends! To Mona for the enjoyable coffee breaks and conversation and to Sharon for being my "mom" and friend at ORNL.

Finally, I'd like to express my gratitude to the National Science Foundation for funding this project and my final year on a research assistantship. It's amazing how much research can be accomplished when teaching is no longer required.

Abstract

Diamond films were grown with various morphologies in a hot filament chemical vapor deposition reactor equipped to monitor the gas phase chemistry. The reactor provided for orifice sampling of gases in the immediate vicinity of the diamond growth surface for introduction into a time-of-flight mass spectrometer. Electron impact ionization was utilized to investigate stable species present during growth. Resonance enhanced multiphoton ionization was employed for the detection of radicals including atomic hydrogen and methyl radical. Measurements were made of the filament and substrate temperature dependence of the H, CH_3, CH_4, and C_2H_2 relative concentrations. Scanning electron microscopy and Raman spectroscopy were used to verify the quality of diamond produced.

Table of Contents

CHAPTER	PAGE
1. Introduction	1
2. Diamond Deposition Technology and Gas Phase Diagnostics	6
Introduction	6
Chemical Vapor Deposition Methods	6
Thermal CVD Methods	8
Plasma CVD Methods	13
Combustion CVD Methods	21
Gas Phase Diagnostics	23
Physical Methods	25
Sample Extraction Methods	26
Optical Methods	28
Summary	33
3. Experimental Instrumentation	34
Introduction	34
Growth Chamber	34
Time-of-Flight Mass Spectrometry	42
Electron Gun Operation	43
Laser	44
Film Characterization	45
Scanning Electron Microscopy	45
Raman Spectroscopy	46
Summary	49
4. Results and Discussion	50
Introduction	50
Electron Impact Ionization	51
Resonance Enhanced Multiphoton Ionization	58
Atomic Hydrogen	60
Methyl Radical	63
Film Growth	70
Conclusions	78
References	82
Appendix	88
Vita	91

List of Tables

Table		*Page*
1.1	Selected properties of diamond	1
1.2	Potential application areas for diamond thin films	4
2.1	Filaments for diamond synthesis	10
4.1	Diamond film growth conditions and resulting α values	71

List of Figures

Figure		*Page*
2.1	Schematic diagram of a hot filament deposition reactor	9
2.2	Schematic diagram of a plasma jet deposition system	12
2.3	Schematic diagram of a microwave plasma reactor	16
2.4	Schematic diagram of a DC plasma reactor	18
2.5	(a) Schematic of an inductively coupled RF plasma CVD reactor. (b) Schematic of a parallel plate, capacitively-coupled RF PECVD reactor	20
2.6	Schematic diagram of a combustion deposition system	22
2.7	Generalized schematic of the processes in a diamond CVD reactor	23
3.1	(a) Schematic of the HFCVD system	35
	(b) Geometry of HFCVD reactor with orifice sampling	36
3.2	Detail of filament assembly and quartz tube support	38
3.3	Mo heater/nozzle for orifice sampling with detail of the press fit aperture	40
3.4	Raman spectra for (a) natural diamond, (b) highly oriented pyrolytic graphite (HOPG), (c) diamondlike carbon, and (d) diamond film	48
4.1	Dependence of the Ne EI signal on substrate temperature. Curve shows a fit to a T^{-1} variation expected due to an ideal gas expansion	52
4.2	(a) Raw data for varying T_s with T_f = 1890 °C. (b) Normalized data to m/z = 20	53
4.3	Substrate temperature dependence of (a) He and (b) Ar signals, normalized to Ne (m/z = 22)	55
4.4	Electron impact ionization of methane and acetylene verses filament temperature with T_s = 780 °C. Films were grown at A, B, and C	57

4.5 Substrate temperature dependence of methane and acetylene with (a) T_f = 1890 °C and (b) T_f = 1420 °C, normalized to m/z = 20 .. 59

4.6 Energy level diagram for atomic hydrogen illustrating the (2+1) REMPI transition observed in this work 61

4.7 Wavelength dependence of the H (2+1) REMPI signal at 243.13 nm 61

4.8 Dependence of H REMPI signal on filament temperature with T_s = 730 °C 62

4.9 Dependence of H REMPI signal on substrate temperature with T_f = 1890 °C 64

4.10 Correlation diagram between united atom, fluorine, and the D_{3h} symmetry orbitals of methyl radical. Arrows indicate the two photon transition observed in this work 66

4.11 The (2+1) REMPI signal of CH_3 66

4.12 Mass spectra of expansion gases under diamond growth conditions with laser tuned on and off the (2+1) REMPI wavelength for CH_3 67

4.13 Dependence of CH_3 REMPI signal on filament temperature with T_s = 730 °C 68

4.14 Dependence of CH_3 REMPI signal on substrate temperature with T_f = 1890 °C 69

4.15 Face centered cubes illustrate the (100), (111), and (110) faces 71

4.16 Cubo-octahedral shapes reveal the growth rate ratios on the <100> and <111> axes. The $\upsilon_{100}/\upsilon_{111}$ is given below each shape ... 72

4.17 SEM images of single crystals. (a) T_f = 1420 °C, T_s = 780 °C; (b) T_f = 1670 °C, T_s = 780 °C; (c) T_f = 2110 °C, T_s = 780 °C; (d) T_f = 1670 °C, T_s = 515 °C 73

4.18 Raman spectra of CVD films. (a) T_f = 1420 °C, T_s = 780 °C; (b) T_f = 1670 °C, T_s = 780 °C; (c) T_f = 2110 °C, T_s = 780 °C; (d) T_f = 1670 °C, T_s = 515 °C 76

List of Abbreviations

BBO	β-BaB_2O_4 crystal
CARS	coherent anti-stokes Raman scattering
CVD	chemical vapor deposition
DC	direct current
egun	electron gun
FTIR	Fourier transform infrared spectroscopy
GC	gas chromatography
HFCVD	hot filament chemical vapor deposition
HPHT	high pressure high temperature
IR-DLAS	infrared diode laser absorption spectroscopy
LIF	laser induced fluorescence
LP	Langmuir probe
MCP	multichannel plate
MI-FTIR	matrix isolation Fourier transform infrared spectroscopy
MS	mass spectroscopy
OES	optical emission spectroscopy
PECVD	plasma enhanced chemical vapor deposition
REMPI	resonance enhanced multiphoton ionization
RF	radio frequency
SEM	scanning electron microscopy
TC	thermocouple

T_f	filament temperature
THG	third harmonic generation
TOF	time-of-flight
T_s	substrate temperature
UV	ultra violet

Chapter 1

Introduction

Diamond is one of the most prized of all materials. Choose virtually any characteristic property of a material and the value associated with diamond will represent the foremost position among all materials considered for that property. Table 1.1 provides a listing of some the material properties that render diamond so useful across numerous fields of science. In spite of these and other useful properties, diamond has never achieved general use in a wide variety of applications due to high cost, limited availability, lack of control over material properties, and limited macroscopic morphologies.

Table 1.1: Selected properties of diamond

Property	**Diamond**	**Comparisons or Comments**
Chemical Reactivity	Extremely Low	
Density (g/cm^3)	3.5	Cu: 8.9; BeO: 3.1; Al: 2.6
Hardness (kg/mm^2)	9000	CBN: 4500; SiC: 4000
Thermal Conductivity (W/cm °C)	20	Ag: 4.3; BeO: 2.2; Cu: 4.0
Tensile Strength (10^6 psi)	0.5 (natural)	304 S/S: 0.85
Compressive Strength (10^6 psi)	14 (natural)	SiO_2: >160
Thermal Expansion Coeff. (10^6 °C^{-1})	0.8	SiO_2: 0.5
Refractive Index (@ 590 nm)	2.41	Glass: 1.4 -- 1.8
Coefficient of Friction	0.05 (dry)	Teflon: 0.05
Transmissivity	225 nm -- far IR	Widest Known
Young's Modulus (GPa)	1030	SiC: 410; Si_3N_4: 310; Si: 140

Some of these drawbacks were addressed by the development of high pressure, high temperature (HPHT) diamond synthesis. This technique allows single synthetic crystals to have dimensions of up to a few millimeters on a side. Some impurities can be controlled and for some types of crystals, the cost can be reduced greatly from the cost of natural diamond crystals. HPHT diamond is very similar to natural diamond in terms of the applications for which it is used. Its relatively low cost has led to its widespread use as a grit material.

The first successful, reproducible diamond synthesis by any method was achieved by William G. Eversole of the Union Carbide Corporation in 1952 using low-pressure chemical vapor deposition (CVD).[1] Since the discovery of CVD diamond, hundreds of researchers have reproduced the process in search of the growth mechanism and the improvement of film characteristics. Many different methods have been successfully employed in the CVD growth of diamond, including thermal, plasma, and combustion systems. These are reviewed in Chapter 2. CVD provides promise for the use of diamond in products which could not have hoped to take advantage of its properties when only natural or HPHT crystals were available. CVD has the potential of controlling diamond film properties and characteristics as well as coating large areas.

One of the most extraordinary aspects of CVD diamond growth is that it takes place under temperature and pressure conditions for which graphite is the

stable state; therefore, kinetics, rather than thermodynamics, determine the bonding in the films. Energy sources provide the necessary activation of the gas phase to generate the species used in the formation of the sp^3 diamond bonds in the deposited carbon film. An understanding of the energy source, resultant deposition chemistry, and the formation of diamond must be obtained to enable control over the deposition process.

Diamond films range from thin films (up to several micron thickness) in either coated or free-standing membranes to thick ceramic plates up to several hundred microns thickness from which products can be laser machined. Deposition areas and rates depend on the deposition method. Areas range from 1 - 100 cm^2, while growth rates are typically 1μm/hr. A vast array of potential applications (see Table 1.2) represents a large driving force toward the development of a reliable, reproducible, effective method for the growth of high quality diamond films. In spite of the twenty five years that have passed since the discovery of CVD, few genuine diamond products have reached the marketplace. CVD diamond has been utilized in X-ray window applications.[2] The slow development is an indicator of the lack of understanding the deposition process and the empirical rather than fundamental approach most researchers have brought to diamond technology. At this time, it is still difficult for most researchers to produce a film of desired quality across a useful substrate area at an economical growth rate. Predicting the film quality in terms of bonding states, impurities, defect concentrations, and morphologies is also a problem. An improved control of the deposition process must be

obtained through an understanding of the basic phenomena (gas phase vs. surface chemistry) responsible for the deposition environment and resulting film characteristics.

Table 1.2 Potential application areas for diamond thin films.

Diamond Property	Application Area
Low Chemical Reactivity	**High Performance Materials** Ceramics, Abrasives, Armor
Hardest Known Material Highest Tensile & Compressive Strength Low Thermal Expansion	**Tooling** Machine Tool Bits & Blades Grinding Tools, Wear Coatings
Extreme Heat Conductivity Excellent Electrical Insulator	**Electronic Substrates & Heat Sinks** Circuit Packaging, High Power Device Heat Sinks
p- and n-type Semiconductor Wide Band Gap Existing Metallization Methods	**Semiconductor Devices** Junction Devices, Bulk-Effect Devices
Excellent Transparency High Refractive Index	**Optical and Electro-Optic Materials** Windows, Coatings Electro-Optic Devices

Once good quality diamond films can be reproducibly deposited, other critical issues can be addressed. One of the most important of these issues involves the scaling of the process from approximately 1 cm^2 to at least 100 cm^2 with uniform thickness, morphology, and bonding state across that area. Significant engineering tasks remain after suitable diamond is reliably produced. The diamond must be machined into the desired shape and size and often polished on one or more surfaces. Further characterization of the diamond film, including film resistivity, thermal conductivity, and impurity concentration, may be necessary depending on the desired application. The

expeditious development of specific diamond-based applications will be through an improved understanding of the physical and chemical phenomena associated with the diamond deposition process itself.

In this thesis, the diamond deposition process was characterized and related to the gas phase composition and resulting film quality. Experimental work required improvements to an existing hot filament CVD reactor, determination of diamond growth conditions, analysis of the gas phase diagnostics during deposition, and characterization of the resulting diamond films. Orifice sampling was employed as a means of probing the near surface region during the deposition process. Electron impact (EI) ionization mass spectrometry was utilized to detect the dominant, stable hydrocarbon species. Radical species, H and CH_3, were monitored using resonance enhanced multiphoton ionization (REMPI) mass spectrometry. Both EI and REMPI measurements were obtained as functions of filament and substrate temperatures.

Chapter 2

Diamond Deposition Technology and Gas Phase Diagnostics

2.1 Introduction

The synthesis of diamond thin films can be accomplished through a variety of CVD methods. One commonality in these methods is that the source carbon is activated in the gas phase. Diamond is deposited on a substrate surface only under a limited range of conditions. In order to understand how these conditions affect the concentrations of activated species and therefore the mechanism(s) for diamond growth, analysis of the environment in the CVD process is necessary. Numerous diagnostic techniques have been employed to study the chemical species present in the gas phase and to measure temperature distributions in deposition chambers. These are reviewed in this chapter.

2.2 Chemical Vapor Deposition Methods

Most CVD methods for diamond growth share the following similarities:

1. The gas phase must be activated with high temperature and/or by plasma excitation.

2. A hydrocarbon species must be present in the gas phase.

3. A species which etches graphite and/or suppresses gaseous graphite precursors (e.g. polycyclic aromatic hydrocarbons) must be present in sufficiently high concentrations. Usually this

species is H, however, O, H_2, OH, O_2, and F_2 have been proposed as additional graphite suppressors.[3,4]

4. The substrate surface must be predisposed to support the nucleation and growth of diamond from the vapor phase. This means the substrate surface should be at or near the solubility limit for carbon in order to support the deposition of diamond on the surface instead of the diffusion of carbon into the substrate. Additionally, the surface of the substrate must not include any catalysts which promote the formation of graphite.

5. A driving force to transport the activated carbon species from the gas phase to the surface of the substrate must be present. Typically this force is simply a temperature gradient allowing for diffusion from the hotter gas phase to the substrate surface. Transport can also be enhanced by application of electrical field.[5]

A wide variety of techniques can be employed to generate these conditions. The absence of one of the conditions described above typically results in the deposition of some non-diamond carbon.[6]

In thermal CVD systems, a hot filament, arc jet or plasma torch provides the energy necessary to activate the gas mixture in order to deposit films. In plasma CVD systems, the plasma source is the activating element. Microwave, direct current and radio frequency plasmas have all been used to produce diamond films. The activation can also be achieved by combustion, typically utilizing an oxy-acetylene torch.

2.2.1 Thermal CVD Methods

2.2.1.1 Hot Filament CVD

Matsumoto et al. first proposed the hot filament CVD process in 1982.[7,8] A schematic of a hot filament CVD reactor (HFCVD) is shown in Figure 2.1. In this method, a hot filament activates a mixture of CH_4 and H_2 that is typically metered into a deposition chamber utilizing flow meters and a throttle valve. Pressures in the chamber are usually 20 to 100 Torr. The substrate is located close (< 1 cm) to the filament to allow for diffusion of the activated species to the surface. A substrate heater can be employed to permit independent control of the substrate temperature.

In general, it has been learned that the hot filament dissociates H_2 into H. The H reacts with the input hydrocarbon, typically CH_4, to form hydrocarbons, e.g. C_2H_2 and CH_3, in the gas phase. All the process parameters for diamond growth in a hot filament CVD reactor are highly interrelated. Relevant process parameters include: filament material, filament temperature, input gas and concentration, substrate temperature, and filament to substrate distance. Because of its simplicity, comparatively low capital and operating cost, filament assisted CVD has become popular in industry where it is imperative to minimize cost per μm of synthetic diamond coating. It is also readily scalable to larger area substrates.

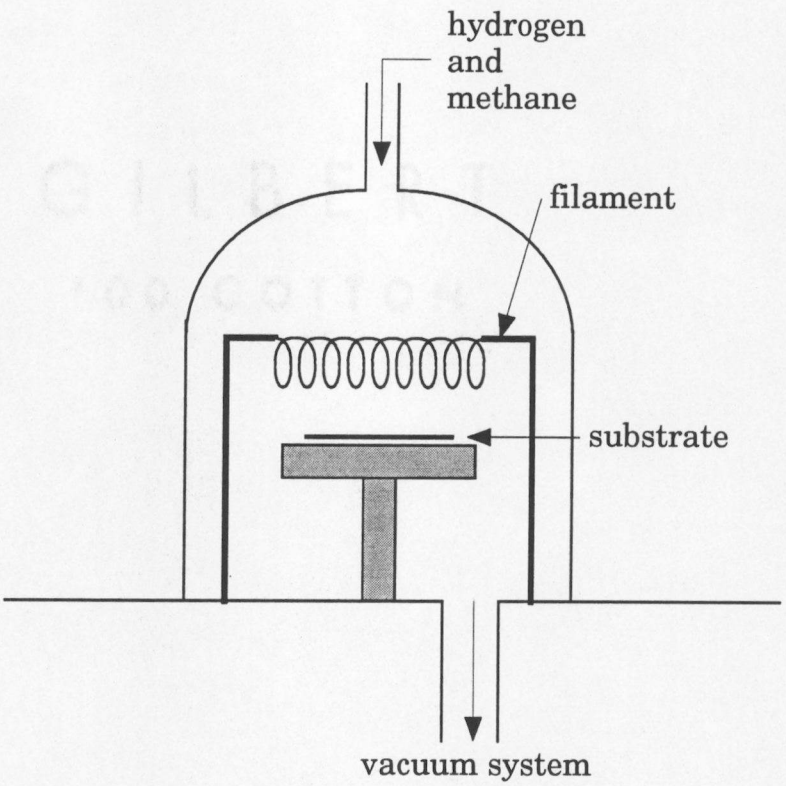


Figure 2.1 Schematic diagram of a hot filament deposition reactor.

Various materials have been utilized for the filament. There are constraints on the electrically conductive refractory materials that can be used for diamond deposition filaments. First, the melting point of the material must be higher than the operating temperature. Secondly, the binary eutectic temperature of carbon and the filament material must exceed the operating temperature to prevent melting or breakage of the filament. Thirdly, the evaporation rate must be considered. Table 2.1 compares the relevant parameters for various filament materials.[9]

Table 2.1: Filaments for Diamond Synthesis

Material	**Melting Point (°C)**	**Evaporation Rate (g/cm^2-s)**	**Carbon Eutectic Point (°C)**
Tungsten	3387	10^{-9}	2475
Carbon	3727	$6x10^{-8}$	3727
Rhenium	3180	$7x10^{-5}$	2486
Tantalum	2996	10^{-8}	2800
Molybdenum	2610	$4x10^{-7}$	2200

While a C filament satisfies the melting point and eutectic-point requirements, it does not produce CVD diamond because the H that forms on a C filament reacts with the C and releases a hydrocarbon species into the gas rather than H. Without H at the substrate, graphite is deposited instead of diamond. Mo is a poor choice because the hot spot on the filament may rise above the eutectic point, causing the filament to melt and fail before the filament is fully carburized.

In the early 1900's, Langmuir discovered that a hot W filament could dissociate H_2 into H.[10,11] During diamond deposition, the W filament reacts with the CH_4 and undergoes carburization (conversion to tungsten carbide). This process affects the structure and microstructure of the filament and influences the nucleation process of the diamond films. After carburization, the filament becomes very brittle and is extremely fragile and difficult to work with. For this reason, other refractory metals were explored for use as filaments.

Singh et al. reported the use of Ta as an alternative filament. Ta produced diamond films similar to those produced by W. Pt filaments heated close to its volatilization temperature of 1300°C produced only graphite deposits.[12] Re was reported by Jasen et al. as an alternative filament.[13] Re does not form carbides upon reaction with hydrocarbons as W does. However, Re does dissolve large amounts of carbon causing the Re filament to swell. This causes the filament to become slightly brittle but not to the extent of the W filaments. Re, unfortunately, is 20 - 100 times more expensive than Ta or W.

2.2.1.2 Arc Jet and Plasma Torch CVD

Arc jets and torches are generally operated at atmospheric pressure. A schematic of a typical plasma jet is shown in Figure 2.2. These systems employ very high power density electrical discharges in high velocity gas streams. Plasma torches can have DC, RF, or microwave power sources.

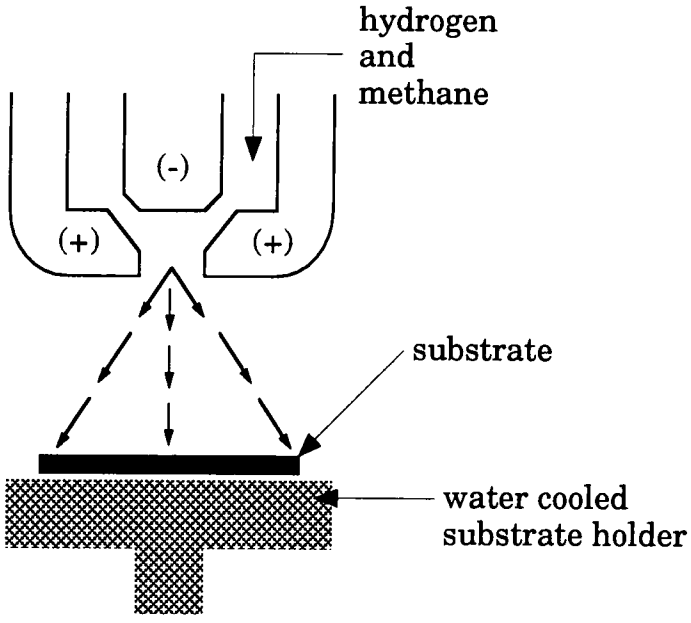


Figure 2.2 Schematic diagram of a plasma jet deposition system.

RF and microwave systems do not have discharge electrodes and therefore have increased lifetimes and improved film purity whereas DC systems are low cost and simple to setup. These methods achieve high growth rates, however, the films often develop voids and defects due to these rates.

Thermal control of deposition substrates is difficult due to the large heat inputs from the arc. For example, a 10″ diameter plasma torch (Tafa Corporation Model 69) transfers over 10^6 W of RF energy to the gas stream, much of which reappears as heat at the stream impingement area. For this reason, expensive and elaborate deposition equipment is often required for the removal of hundreds of kW of heat from the deposition substrate. An additional expense associated with arc jet systems is that of gas consumption due to the large flow rates.

2.2.2 Plasma CVD Methods

Various types of plasma assisted CVD methods for diamond growth exist. Plasmas are generated by electrical discharges or by induction heating. The plasma creates H and C precursors essential for diamond growth. Efficiencies differ depending on the type of plasma.

In plasmas exposed to high electric fields, H is produced by electron impact dissociation of H_2. Although the dissociation energy of H_2 is 4.5 eV, the

electron impact dissociation of H_2 requires electrons with energies above 9.5 eV and dissociation reaches a maximum at electron energies of 25 eV. Consequently, the H produced in plasmas has a very high kinetic energy since the difference between the dissociation energy and the electron impact energy must be taken up by the kinetic energy of the H. Atomic hydrogen produced by thermal methods has low kinetic energy since it is formed by a direct transfer of thermal energy that breaks the H_2 apart without imparting additional excess energy that would appear as the kinetic energy of the H product.[9]

The pressure of the plasma determines the absolute concentrations of atomic hydrogen and neutral radicals . In low pressure plasmas, the electrons gain high kinetic energies from the electric field. The electrons are not able to transfer the majority of this energy to molecular species due to the long mean free path. The resulting gas temperature is low compared to that of the electrons. Atomic hydrogen and neutral species are therefore produced in low concentrations with only high energy electrons. In high pressure plasmas, the gas and electron temperatures are relatively the same due to the short electron mean free path. Both electron and molecular collisions contribute to the formation of H and neutral radicals thus increasing their relative concentrations. The increased concentrations of growth species in high pressure plasmas leads to improved growth rates for these systems.

2.2.2.1 Microwave Plasma CVD

Microwave plasma CVD is the most widely used method for the growth of diamond films. A schematic of a typical microwave reactor is shown in Figure 2.3. The total pressure is typically 5 to 100 Torr, with a microwave power of 100 to 700 W, a substrate temperature of 700 to 1000 °C and 0.5 to 2% CH_4 in H_2 gas mixture. Oxygen is frequently added to improve growth rates and reduce substrate temperatures for diamond growth. Microwave plasmas are different from other plasmas in that the microwave frequency can oscillate electrons. Collisions of electrons with gas atoms and molecules generate high ionization fractions. Microwave plasmas are typically described as having hot electrons and cool ions and neutrals. Microwave CVD for diamond differs from other microwave processes which are operated at one Torr or less.

There are numerous advantages to microwave deposition when compared to other methods of CVD. The plasma is confined to the center of the deposition chamber in the form of a ball, thus preventing carbon deposition on the walls of the quartz tube. The discharge has a higher frequency than RF plasmas and consequently produces a higher plasma density with higher energy electrons. Another advantage is that microwave chambers do not have electrodes and hence avoid film contamination due to erosion of the electrodes.

Stoner et al. reported an enhancement in the nucleation density of microwave plasma CVD diamond when a negatively biased silicon substrate was used.[14] Diamond has also been deposited when a magnetic field was coupled to a

microwave reactor. This combination can also cause an electron cyclotron resonance when the pressure in the chamber is below 10 mTorr allowing the mean free path of the electrons in the plasma to be long enough to oscillate in the magnetic field.[15]

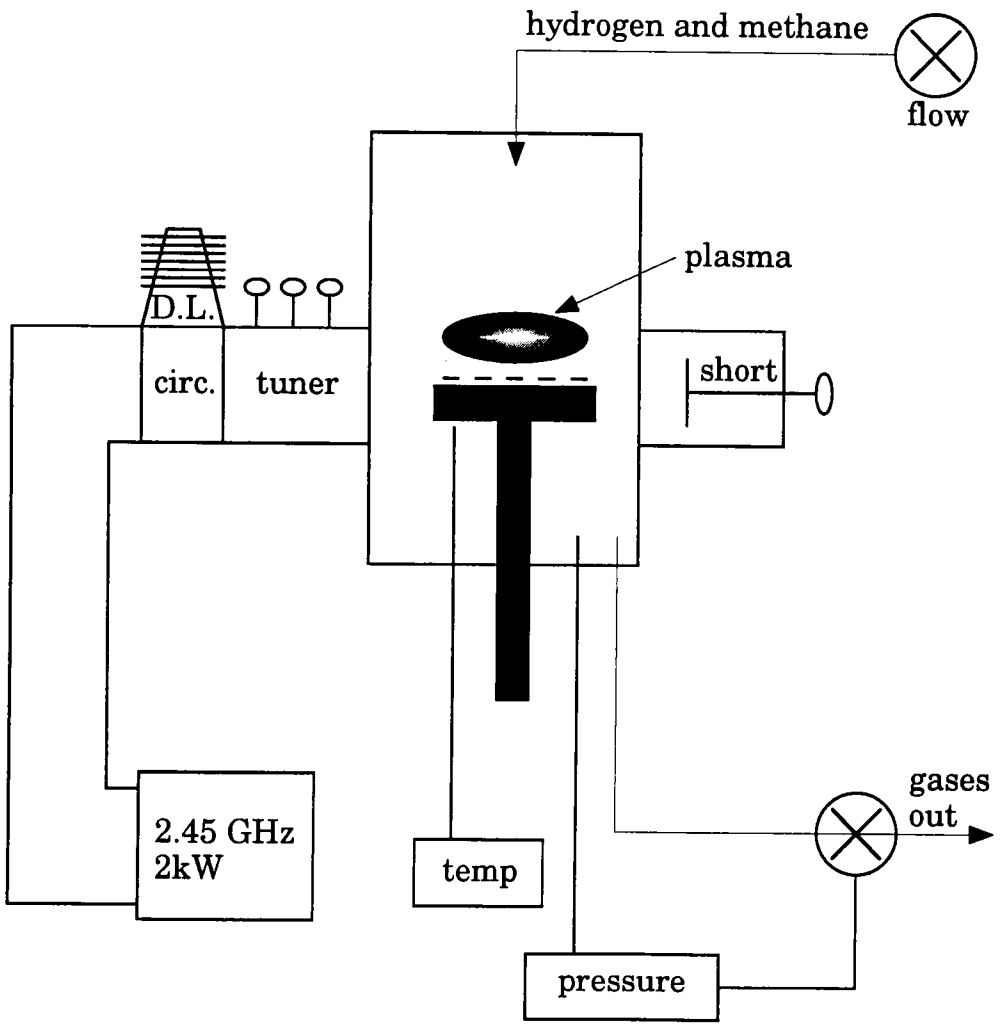


Figure 2.3 Schematic diagram of a microwave plasma reactor.

2.2.2.2 Direct Current Plasma CVD

Low (1 - 4 A) direct current (DC) plasmas are perhaps the simplest of the diamond producing technologies, although the difficulty in maintaining stable discharges and low growth rates has limited their utilization. Diamond films produced by DC plasmas contain higher concentrations of hydrogen and are under increased stress. They may contain impurities from the erosion of the electrodes. A schematic of a DC plasma system is shown in Figure 2.4. A plasma in a hydrocarbon-H_2 mixture is excited by applying a DC bias across two parallel plates, one of which is the substrate. The substrate can be either the cathode or the anode. The reaction gas is fed through the electrode opposite to the substrate. When the substrate is the anode, it is heated by electron bombardment to approximately 800 °C. Lower substrate temperatures can be obtained by cooling the back of the substrate with water. A total pressure of 200 Torr and discharge parameters of 1000 V and 4 A/cm^2 are typically used. In cathodic films, operating pressures are reported to be 5 to 30 Torr with charged particle flow to the substrate of 10 to 20 mA/cm^2.

DC plasmas require conducting or semiconducting substrates since the substrate is part of the plasma electrical circuit. However, diamond is generally an effective insulator so it is somewhat surprising that it can be grown in this system. A few theories have been proposed to explain the apparent conductivity of the films in the plasma environment. The most feasible is that the hydrogen present in the growth environment interacts with other impurities and defects in the diamond to produce a semiconducting

diamond.[16] A second effect may be that the ultraviolet light generated by the plasma induces photoconduction.

Engineering advantages of DC plasmas for diamond CVD include ease in scaling to large areas, relative insensitivity to gas dynamics, and the production of fine grain films in comparison to most other CVD methods.[17]

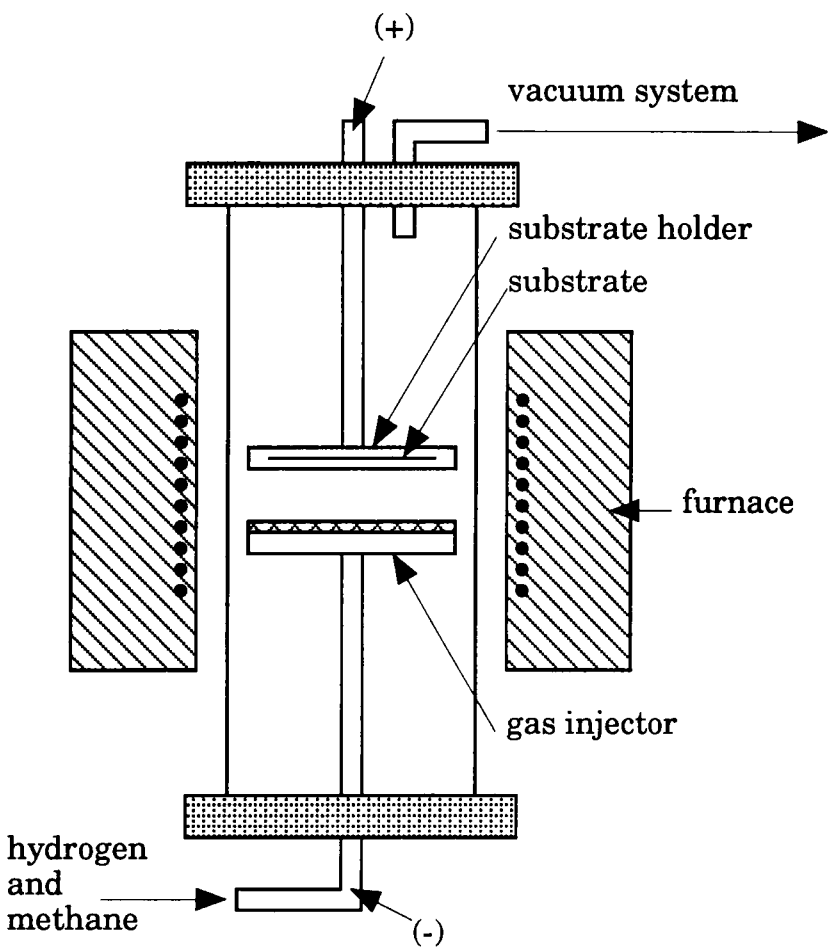


Figure 2.4 Schematic diagram of a DC plasma reactor.

2.2.2.3 Radio Frequency Plasma CVD

Radio frequency (RF) power can be applied to create a plasma in two electrode configurations: capacitively coupled parallel plate and induction. Schematics of these two reactor types are illustrated in Figure 2.5. Typical conditions include 0.5 to 2% CH_4 /H_2 gas mixture, 1 to 30 Torr total pressure, 800 to 1000 °C substrate temperature, and a RF power of 500 to 1000 W.

Higher power RF plasmas generators are necessary to dissociate hydrogen and initiate diamond growth. Increasing the power is also believed to increase the electron densities.[9] Disadvantages of using high power discharges include sputtering from the walls of the silica tube and contamination of the diamond films with silicon carbide.

An advantage of RF plasmas is that they can be easily generated over much larger areas than microwave plasmas. RF plasma CVD diamond films typically have small crystal grains and good adhesion to a variety of substrates. Homoepitaxial diamond films have been grown by RF induction plasma enhanced CVD.[18] Roman and Colket have used RF induction plasma to deposit polycrystalline diamond while preforming in-situ gas phase laser spectroscopy. They utilize coherent anti-stokes Raman scattering, CARS, to sample the plasma as a function of distance away from the substrate surface.[19] Matsumoto described the synthesis of 20 mm diameter diamond films at a growth rate of 120 μm/hr in an RF generated thermal plasma at atmospheric pressure.[20]

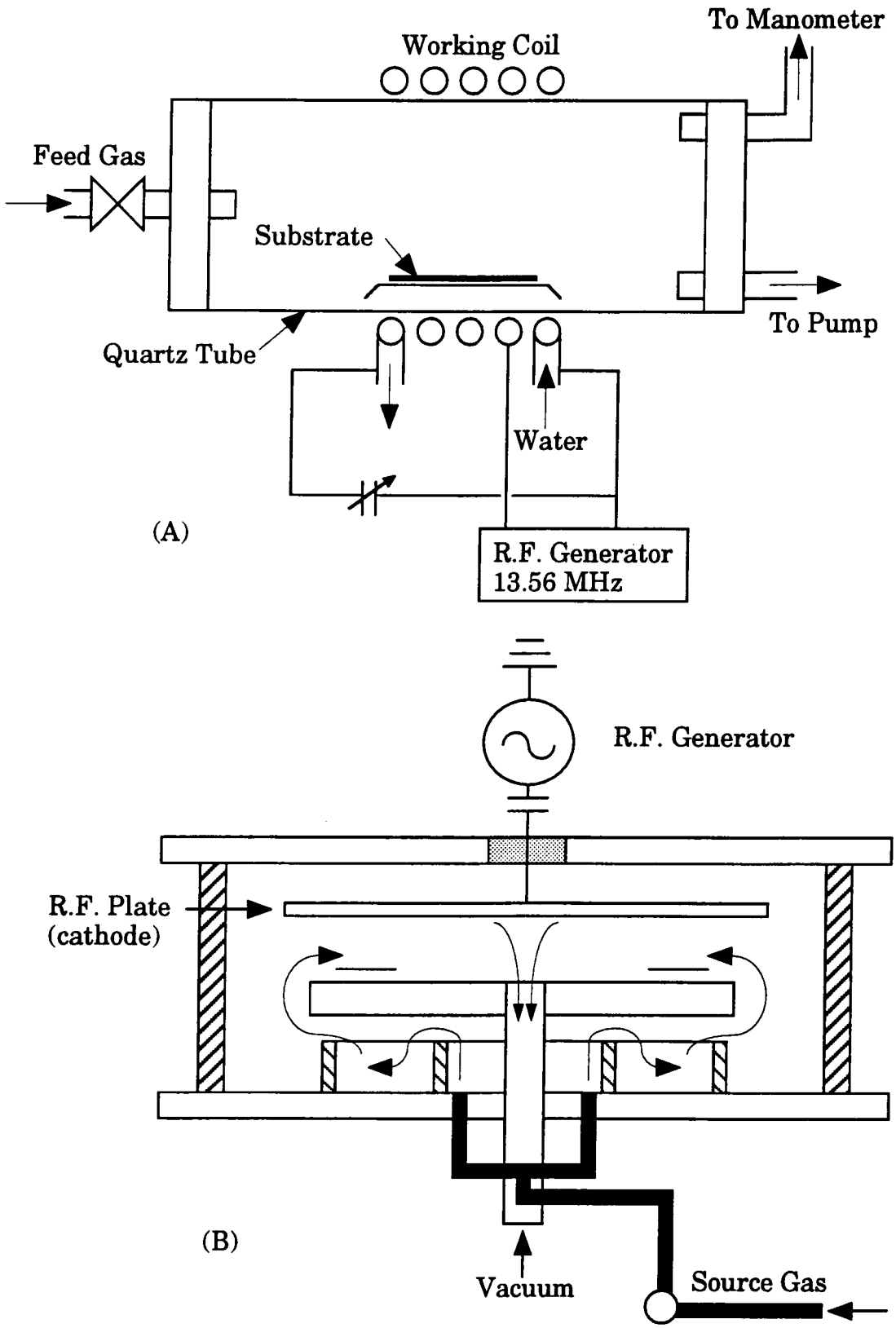


Figure 2.5 (A) Schematic of an inductively coupled RF plasma CVD reactor. (B) Schematic of a parallel plate, capacitively-coupled RF PECVD reactor.

2.2.3 Combustion CVD Method

Hirose et al. announced the deposition of diamond particles by combustion in the Spring of 1988. They placed the flame of an oxy-acetylene welder's torch onto a substrate in room air. Diamond particles were deposited beneath the center of the flame. A schematic of a combustion apparatus in shown in Figure 2.6. In their work, an ordinary welder's torch with a brazing tip (which burns approximately a 1:1 mixture of C_2H_2 to O_2) was placed in contact with a cooled surface between 800 and 1050 °C and diamond crystals were observed to nucleate and grow.[21]

Combustion CVD is appealing because it is typically performed at atmospheric pressure and lends itself to low cost, high volume applications. There are significant engineering challenges for scaling up combustion deposition. Heat inputs to substrate materials are extremely high with oxy-acetylene flames and control of the substrate temperature is difficult to achieve. Boundary layer effects become important in determining deposition rates and quality uniformity. Finally, flame deposited films often contain internal voids, or areas of incomplete coalescence, which appear to be a consequence of very rapid growth. It may be possible to avoid this problem by using a cyclic growth system in which diamond is deposited for a short time, then the fuel mixture is changed so that etching of nondiamond-bonded carbon occurs, followed by another deposition stage, leading to a highly diamond bonded film.[22]

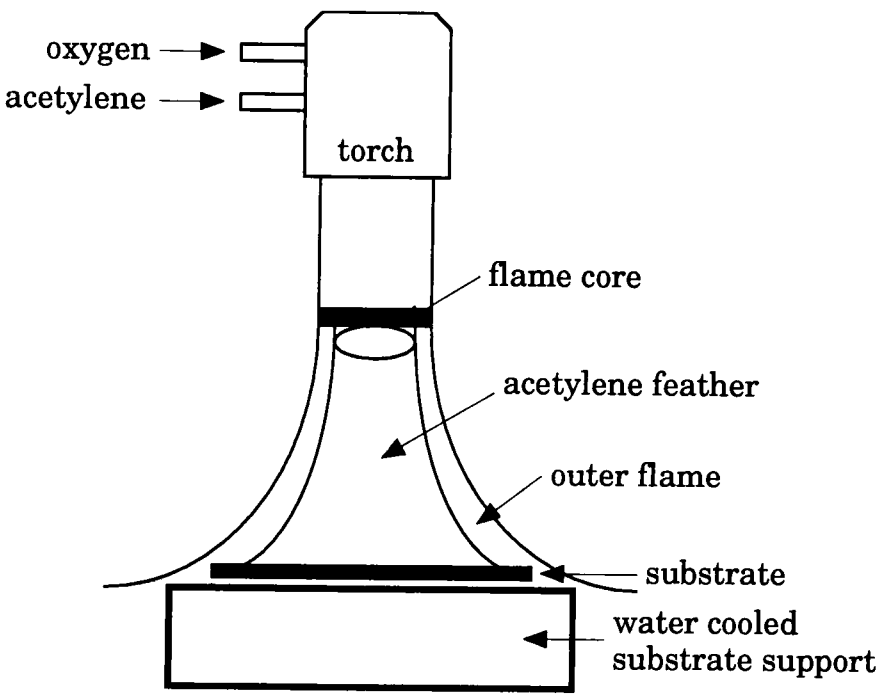


Figure 2.6 Schematic diagram of a combustion deposition system.

2.3 Gas Phase Diagnostics

The chemistry occurring in the gas phase is a key component to the understanding of the chemical vapor deposition process. In order to understand this process, gas phase diagnostic techniques have been applied to the various deposition methods discussed. Although numerous methods are utilized to deposit diamond, the general characteristics are similar and are depicted in Figure 2.7. [23]

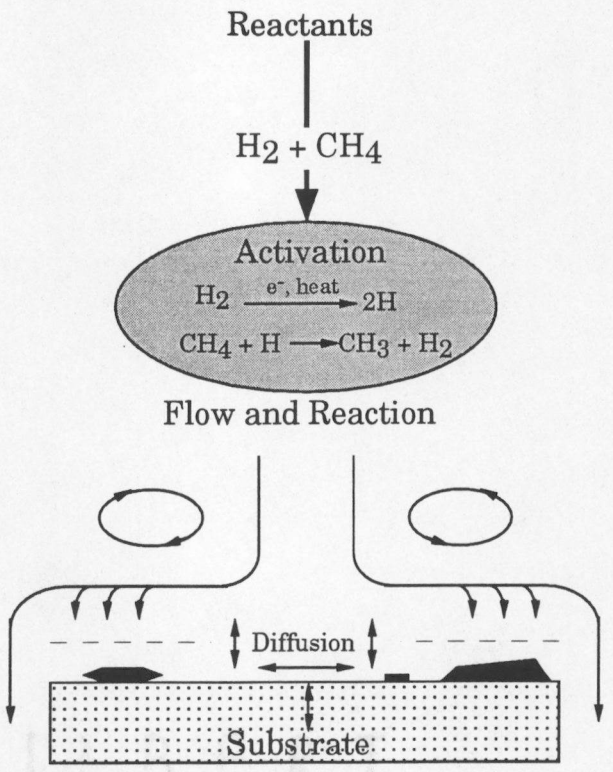


Figure 2.7 Generalized schematic of the processes in a diamond CVD reactor.

The species at the growth surface are determined not only by chemical reactions but also by gas transport in the reactor. Diffusion, convection, and forced flow can carry species through the reactor. Species must pass through a stagnant flow region (the boundary layer) to reach the substrate. On the substrate surface, adsorption, desorption, surface and bulk diffusion, and chemical reactions can all occur. These processes can limit or contribute to diamond growth and their rates depend on the temperature, structure, and composition of the surface.

Gas phase diagnostic techniques can be used to monitor the transport of species to the growth surface and measure their concentrations in the boundary layer. These concentration measurements can then be related to conditions for optimum diamond growth rates and film quality. Quantitative measurements can guide the development of chemical, thermal, and mass transport models and provide experimental verification of the results of theoretical calculations. Gas phase diagnostics will also be valuable for process control and optimization.

The ideal diagnostic technique would be nonintrusive, sensitive, and species selective yet able to detect all species of interest. The technique would also determine the environmental temperature and provide spatially resolved measurements. It should be inexpensive and easy to use with straightforward data analysis. Of course no such technique fulfills all these criteria.

The gas phase diagnostic techniques used in diamond CVD can be divided into three types: physical probe methods, sample extraction methods, and optical probe methods. Physical probe methods introduce a probe into the chamber. Sample extraction methods use ex-situ analysis of an extracted portion of the gas. Optical methods employ photons as a probe of the growth environment.[23]

2.3.1 Physical Methods

Physical methods are intrusive. Electron characteristics or gas temperature can be measured physically with a wire. Langmuir probes (LP) are used to measure the potential, electron density, and electron temperature in plasmas. An insulated wire, with an exposed tip, is placed into the plasma and the current flow is monitored as a function of a bias voltage applied to the probe. Data analysis for a LP is complicated by difficulties in determining the collection area of the probe. The collection area is not the physical area of the collector, but rather the size of the plasma sheath.[24]

Thermocouples (TC) are sometimes used to measure the gas temperature and are often connected to the substrate to obtain an indication of the substrate temperature. In measurement of the gas temperature, the TC and the gas in the immediate vicinity are assumed to be in thermal equilibrium. Heat sources and sinks include: gaseous conduction, radiative heating, conduction through lead wires. The temperature is determined by a balance of heat flow to the tip of the TC. However, if an insulating material is deposited on the tip, the indicated temperature is no longer valid.[23] Placement of the TC on the

substrate so that good thermal contact is achieved is critical if accurate measurements of the substrate temperature are to be obtained.[25]

2.3.2 Sample Extraction Methods

Gas chromatography (GC), matrix isolation Fourier transform infrared spectroscopy (MI-FTIR), and mass spectrometry (MS) are examples of sample extraction methods used in CVD. They have the advantage that many species can be monitored simultaneously, with good sensitivity and resolution. Absolute concentrations can be determined with the use of an internal standard. Stable species are easily monitored by connecting the sampling instrumentation to the exhaust of a CVD chamber. However, these measurements lack spatial selectivity and only provide average reactor gas concentrations. Some spatial selectivity can be obtained by use of a capillary probe which is inserted into the reaction gases.[26,27] These probes have the disadvantage that they can perturb the environment being investigated. and cause a variation in gas velocity, composition, temperature, and pressure. In addition, they have limited value for probing chemically reactive species, such as free radicals, since these species are eliminated or their concentrations altered by reactions at the walls of the probe. Incorporation of an orifice in the growth surface through which the gases can be sampled either in an effusive or molecular flow provides a less intrusive extraction method. Orifice sampling allows both stable and reactive gases present directly above the growth surface (the boundary layer) to be studied.[28]

2.3.2.1 Gas Chromatography

In GC, gas samples pass through a sampling loop and portions are injected into a chromatography column. Quantitative determination of concentrations is simplified because there is usually no fragmentation occurring in the GC.[29] If the chemistry of the probe is well understood, it may be possible to extract information about the radical concentrations from measurements of stable species.

2.3.2.2 Matrix Isolation Fourier Transform Infrared Spectroscopy

MI-FTIR is a combination of sample extraction, isolation in a frozen rare gas matrix, and infrared analysis.[30,31] How the sample is extracted determines if reactive species can be condensed in the matrix. Chu et. al. used a water cooled sampling probe so that recombination and reaction of the radicals occurred in the probe and only stable species were frozen in the matrix.[32] Spectroscopic interrogation of the matrix is similar to gas phase FTIR, but with higher sensitivity due to the quenched rotational motion in the matrix .

2.3.2.3 Mass Spectrometry

MS can measure numerous species simultaneously, rapidly, and easily. Ion fragmentation can lead to difficulties in determining concentrations, but can also aid in the identification of species. A modified sampling technique of molecular beam mass spectrometry allows for the direct detection of radical species. In theory, a second orifice, called a skimmer, and pumping stage forms the gas into a molecular beam. The species undergo a free jet expansion,

which slows reactions immediately after the sampling orifice. Because radicals can be formed during the ionization process, photoionization or threshold ionization is employed. With threshold ionization, the electron impact energy is selected below the ionization potential of the parent molecule, yet above that of the radical.[23] Hsu utilizes this technique to detect CH_3 and H.[33]

2.3.3 Optical Methods

Optical methods can monitor radical species as well as stable molecules. They can determine the identity of compounds through characteristic absorption or emission bands. The temperature of the species can be determined through their internal rotational or vibrational state populations. Optical methods are often the least intrusive diagnostic technique and can be preformed in situ. The perturbation to the growth environment can be minimal. Disadvantages are that they require high photon fluxes or powers which may perturb the gas and short wavelengths or high laser powers can also produce photochemical changes that may alter the environment.

2.3.3.1 Optical Emission Spectroscopy

Optical emission spectroscopy, OES, is a very sensitive technique applicable to a wide variety of fluorescing species. With OES, photons emitted by electronically excited species are detected. It is applicable to systems with sufficient numbers of excited species present, mainly plasmas and flames. Important diamond growth species such as methyl radical, methane, and

acetylene have not been detected by this method because they do not fluoresce efficiently.

OES is simple, inexpensive, and fairly easy to implement. To determine the excited state populations from emission intensities requires detailed information on the radiative and nonradiative processes for each emitting state. To ascertain the total concentration of a species requires further understanding of the excitation process that created the species. In practice it is extremely difficult to relate observed emission intensities to ground state concentrations. Therefore OES data provides an initial, but incomplete, picture of the chemical environment.[23]

2.3.3.2 Laser Induced Fluorescence

Detection of species through fluorescence selectively excited by a laser is commonly referred to as laser induced fluorescence (LIF). LIF is sensitive, selective, and provides spatially resolved detection and temperature determination of species that are difficult to detect with other methods. LIF can be difficult to implement. Most species of interest in diamond CVD have their lowest electronic transitions in the far UV. In order to avoid UV-induced photochemistry, multiphoton excitation is used instead of single photon absorption. These multiphoton processes require high power, pulsed, tunable dye lasers that are focused into the region of interest.

LIF monitors fluorescence from molecules which have been excited to and from

specific internal energy levels. When corrected for excitation transition strength, LIF data can provide a determination of state selective initial populations. Comparison with a Boltzmann distribution allows one to determine whether the system is in thermal equilibrium and if so its temperature. An advantage of LIF is that both concentrations and temperatures can be acquired at the same time with good resolution. Major disadvantages include the small number of species with accessible fluorescence transitions and difficult data analysis.[23]

2.3.3.3 Infrared Absorption

The excitation of vibrational or rotational transitions within a species through the absorption of infrared light provides for excellent identification of the chemical nature of the absorbing species. Both infrared diode laser absorption spectroscopy (IR-DLAS) and Fourier transform infrared spectroscopy (FTIR) have been applied to CVD diamond. Both methods have poor spatial resolution since the IR beam diameter is relatively large (typically 1-10 mm) and absorption is integrated along the entire length of the beam path through the chamber.

Selective and sensitive detection is possible through the use of tunable, single-mode diode lasers.[34] However, the tuning range of diode lasers is limited, and absorptions from different species within the same spectral scanning range of a single diode laser are rarely found. Thus, it is generally not possible to detect more than one component at a time. Ample sensitivity is obtained by

multipass reflection of the laser beam through the chamber. Celii et al. used IR-DLAS to perform the first in situ detection of ground-state gas phase species in a diamond CVD environment.[35]

FTIR allows for the detection of all IR active species in one spectrum.[36] It has less selectivity and sensitivity than IR-DLAS. Minor species can usually not be detected because the beam generally makes a single pass through the chamber. A FTIR spectrum contains contributions from all absorbing species and can become congested in a complex environment. FTIR is relatively easy to implement due to a large analytical technology base and is therefore appealing as a process control technique.

2.3.3.4 Resonance Enhanced Multiphoton Ionization

Resonance enhanced multiphoton ionization (REMPI) is a combination of optical and physical methods because it often requires the introduction of a probe wire for collection of photon-produced charged species. When absorption and ionization are enhanced by a resonance near an integral multiple of the photon energy, the probability of ionization increases dramatically compared to multiphoton ionization (MPI). REMPI is more intrusive than other optical techniques because a probe wire or mass spectrometer is required to collect the generated electrons or ions. It is useful for monitoring species with weak fluorescence, such as hydrocarbons important in diamond growth. Quantitative spatial profiles are difficult to obtain with a wire probe because saturated electron collection must be maintained.[37] This is a problem when

translating the biased probe relative to the other reactor surfaces; therefore, measurements have usually been restricted to fixed probe-substrate separation geometries.

REMPI has been used to detect both H and CH_3 in hot filament CVD reactors. The CH_3 REMPI intensity increased with both the initial reactant CH_4 concentration and the filament temperature.[38,39] Spatial dependence of the intensity was also reported.[38] H was detected using a (3+1) REMPI process. H concentration increased with increasing filament temperature. Measurements above and below the filament indicate that diffusion is the primary transport mechanism for H.[40]

2.3.3.5 Third Harmonic Generation

Third harmonic generation (THG) is a four-wave mixing process. In THG, a single laser frequency drives the process, with enhancement coming from a nearby internal energy level of the species of interest, nearly resonant with three laser photons. Phase matching between the incident laser beam and the third-harmonic beam is allowed because the refractive index at energies above the resonance is negatively dispersed due to the presence of the resonance. Both the intensity and the frequency of the generated third-harmonic light are dependent on the concentration of the species. Celii et. al. have utilized THG in the detection of H in both plasma and hot filament systems.[41]

2.4 Summary

A number of gas activation systems have been shown to produce diamond films. The advantages and disadvantages of each method should be considered for each application. The same is true when determining the gas phase diagnostic tools to utilize. For this work, a hot filament reactor equipped with orifice sampling, thermocouple, and time of flight mass spectrometer was selected. The system provides the ability to perform gas phase analysis (using EI or REMPI) on the orifice sampled near surface gases under conditions which produce diamond film growth.

Chapter 3

Experimental Instrumentation

3.1 Introduction

The goal of this research was to examine the relationship of gas phase species concentrations with diamond film growth parameters and film characteristics. The experiments were performed in a HFCVD reactor equipped with a time-of-flight mass spectrometer for gas analysis. The mass spectrometer was used to monitor the chemical species produced immediately above the diamond growth surface. Ionization of the gases sampled was accomplished with an electron gun (for stable species) or a laser (for radical species). Scanning electron microscopy and Raman spectroscopy were utilized to analyze the diamond film morphology and quality. The chamber is described in §3.2, while the mass spectrometer is discussed in §3.3. Film characterization techniques are detailed in §3.4.

3.2 Growth Chamber

A special HFCVD reactor was designed for gas phase diagnostics during the deposition process. A schematic of the system is shown in Figure 3.1 (a) with the geometry pictured in Figure 3.1 (b). The chamber was divided into three regions: the growth region, the expansion region, and the mass spectrometer. An orifice separated the growth and expansion regions, while a skimmer

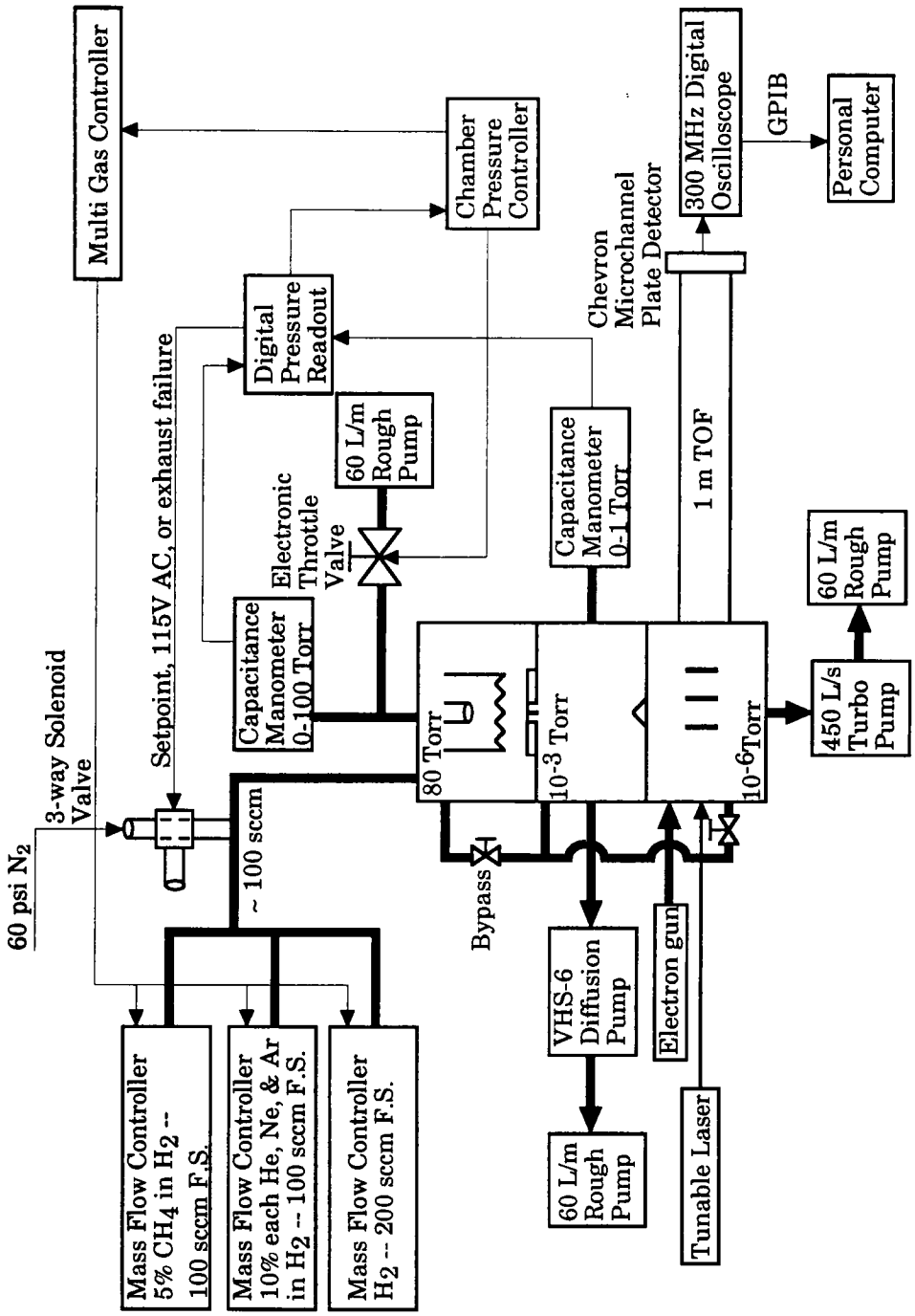


Figure 3.1 (a) Schematic of the HFCVD system.

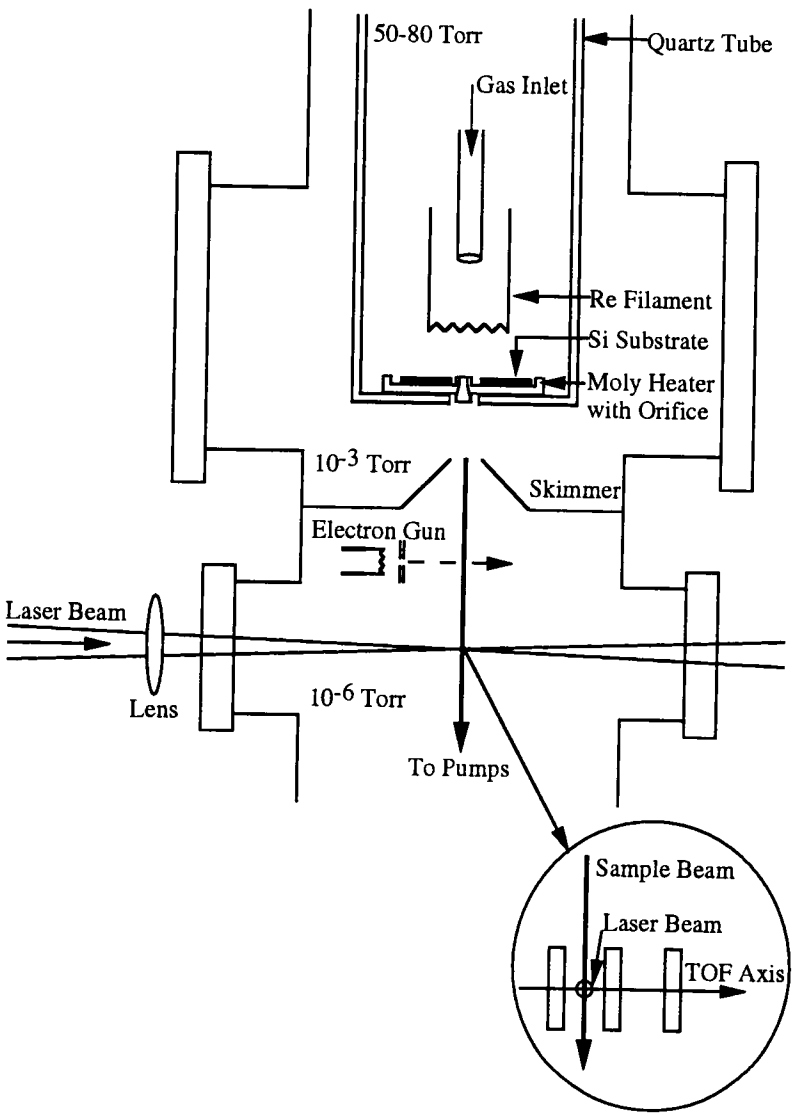


Figure 3.1 (b) Geometry of HFCVD reactor with orifice sampling.

separated the expansion region and the mass spectrometer. A 76 mm diameter quartz tube enclosed the growth region.

Figure 3.2 details the filament assembly and quartz tube support. The quartz tube was held in place by an O-ring compressed between two flanges. Three alignment rods allowed the tube to be translated to align the orifice with the skimmer. Access to the interior of the reactor was via a high vacuum flange that also provided the gas inlet port and heater and thermocouple feedthroughs. The filament consisted of ~15 cm of 0.5 mm diameter Re wire wound 7 to 9 turns in 3.0 mm diameter coils. The filament was connected to W rods that attach to feedthroughs in the top closure flange. The filament was powered by a Sorensen DCR 40-40B power supply. A setting of 20 V and 18 A was typically employed to obtain a filament temperature for diamond growth. The filament brightness temperature was measured through a side arm glass viewport and the quartz tube using a single color optical pyrometer. The indicated temperature was calibrated for the error due to the glass and quartz windows by making temperature measurements of a light bulb outside and inside the chamber. There was a 90 °C difference in the two measurements. The centerline of the filament was typically 20 mm from the gas inlet and 5 to 10 mm from the substrate. The substrates were 2 cm^2 Si wafers, either (111) or (100). They were abraded with 6 μm diamond paste on one-half of the top surface. The wafers were cleaned with methanol in an ultrasonic bath to fully remove the paste. A 3.3 mm hole was drilled through the center of the

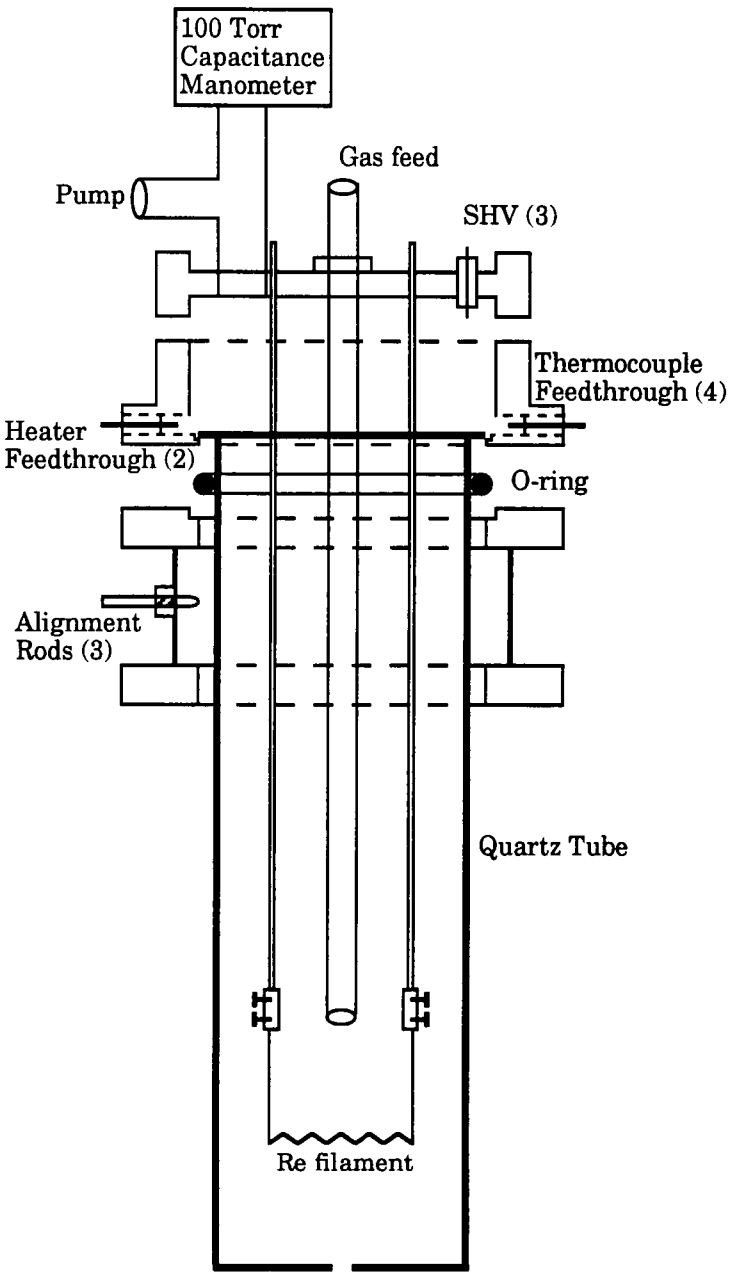


Figure 3.2 Detail of filament assembly and quartz tube support.

substrate so that it fit over the orifice post of the heater/nozzle (see Figure 3.3). This allowed the substrate surface to be flush with the aperture.

Figure 3.3 shows the Mo substrate heater/nozzle. It was inserted into a 6.5 mm hole in the floor of the quartz tube. The heater was designed to provide independent substrate temperature control as well as a uniform lateral temperature. A 200 μm Mo electron microscopy aperture (Ladd Research Industries, Inc., Burlington, VT) was press fit into the heater to provide the nozzle for gas expansion. The aperture mount was elevated to provide a post to hold the substrate. The aperture could be replaced easily to change the orifice diameter in 50 μm increments. Approximately 30% of the inlet gas flowed through the hot orifice for the 200 μm aperture under typical growth conditions and ~10% leaked between the heater and the quartz tube at room temperature. The remaining 60% of the gas flow was exhausted into a rotary pump. The heater was wrapped twice with 0.5 mm Re wire that was encased in alumina beads. The Re wire was attached to W rods that led to feedthroughs in the support flanges of the quartz tube. The heater was powered by a 18 A variac. An indication of the substrate temperature was obtained using a type S (Pt/Pt-10%Rh) TC that was located in a shielded well in the heater beside the substrate.

Constant mass flows of CH_4, H_2, and a noble gas mixture of He, Ne, and Ar in H_2 were metered by a multichannel gas controller (Model 147B, MKS Corporation, Andover, MA) and mass flow controllers (Model 2259C) into the

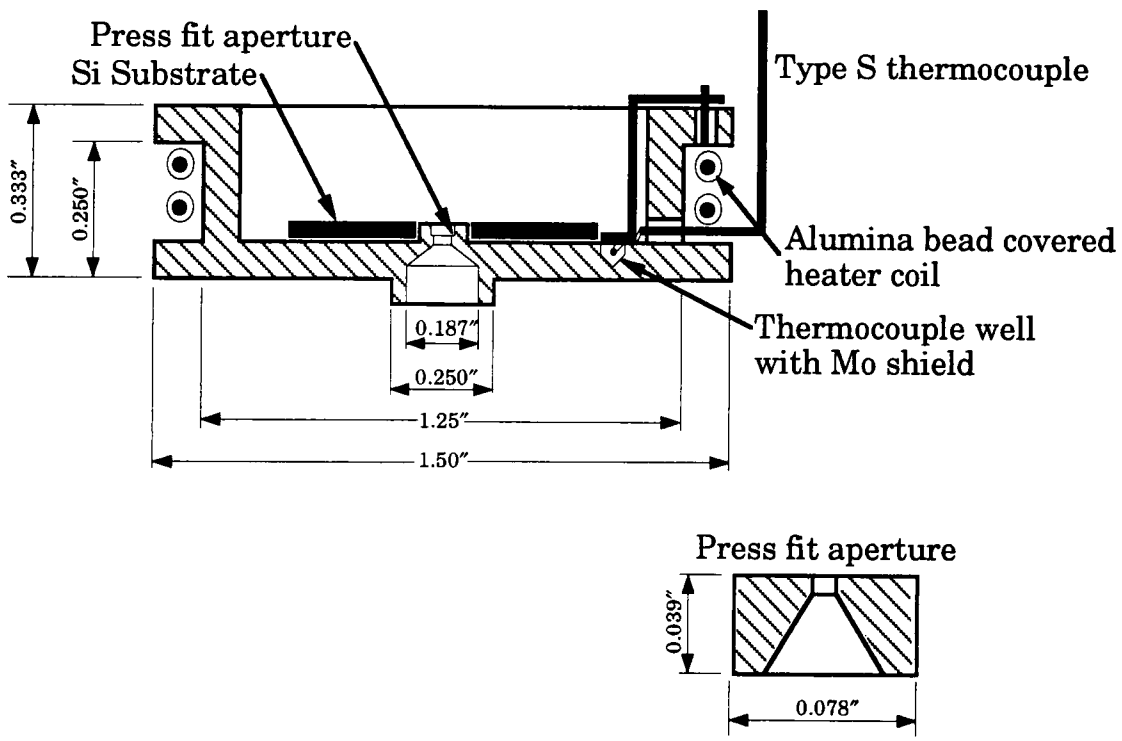


Figure 3.3 Mo heater/nozzle for orifice sampling with detail of the press fit aperture.

chamber at a total flow rate of 100 sccm. The noble gases were present to provide an internal standard by which systematic effects were eliminated from the results. They were also used for the calibration of the time-of-flight mass axis for electron impact ionization. The pressure in the growth portion of the chamber was typically 80 Torr, measured using a 1-100 Torr capacitance manometer gauge (Baratron Model 128A, MKS, Andover, MA). The pressure was controlled by a throttle valve and a rough pump.

The expansion region was pumped to a pressure of $1x10^{-3}$ Torr, indicated by a 0-1 Torr capacitance manometer gauge (Baratron Model 128A), using an oil diffusion pump (Model 0184-85826, Varian, Lexington, MA). A conical molecular beam skimmer (0.5 mm diameter) formed the aperture into the high vacuum region ($2x10^{-6}$) of the chamber where time-of-flight mass spectrometry was performed. The skimmer tip was 8 mm from the orifice and 10 cm from the center of the TOF extraction plates. A 450 L/s turbomolecular pump (Model TMP450, Leybold-Heraeus, Germany) (~310 L/s for H_2) maintained the pressure in this region. An ion gauge provided the pressure readings of the mass spectrometer. The system also contained a vacuum bypass consisting of $^3/_8$" polyethylene tubing and 2 valves, installed to connect the three chamber regions to prevent quartz tube breakage during pressurization to and evacuation from atmospheric pressure.

3.3 Time of Flight Mass Spectrometry

The principle of operation of the time-of-flight (TOF) mass spectrometer is very simple. First, ions were produced by bombarding the neutral target gas with a pulsed electron or laser beam. The ions were then accelerated by an electrostatic field and were injected into a field free drift tube. A two stage acceleration region was employed which is commonly referred to as the Wiley-McLaren geometry.[42,43] The ions drifted down the tube until they were detected by an ion multiplier. For a point source, the kinetic energy is the same for all the accelerated ions, and therefore the velocity of each ion is inversely proportional to the square root of its mass. The Wiley-McLaren geometry corrects for variations in ion energy due to finite source size to first order. An ion detector placed at the end of the drift tube detected ions of different masses at different times. A chevron multichannel plate (MCP) detector was chosen because of its multiplicative advantage. A fast timing preamplifier (Model VT120C, EG&G Ortec, Oak Ridge, TN) provided a gain of 20. The record of the detector signal as a function of time may be easily analyzed to obtain the mass distribution of the ion beam using the equation:

$$t = t_0 + \frac{L}{\sqrt{2E}}\sqrt{m}\,.$$

The TOF mass spectrometer utilized in this investigation was a modified commercial spectrometer from The R.M. Jordan Company (Grass Valley, CA).

A digital storage oscilloscope (Model 2432, Tektronix, Inc.) was utilized to digitize the voltage pulse output from the detector. A program written by Prof.

LinJun Wang in Quick Basic transformed the voltage vs. time scans into mass axis vs. intensity plots on an IBM compatible 286 personal computer.

3.3.1 Electron Gun Operation

The electron gun (egun) was used to generate ions in the acceleration region of the TOF mass spectrometer. Electrons of 70 V energy were emitted from the egun into the space between the mass spectrometer repeller plate and extraction grid while both were at the same potential (1800 V). The pulser then momentarily dipped (180 V) the extraction plate to a lower voltage. This withdrew the ions through the extraction grid and into the acceleration region. The ions then drifted down the flight tube to the detector 1 m away. The MCP detector was set to a typical voltage of 2000 V. The repetition rate of the egun was 1 kHz. The egun was typically located perpendicular to the TOF axis. It was connected to the chamber via a 2 $^3/_4$″ flange to make contact with the acceleration plates of the mass spectrometer. This was the same port also used for laser beam optical access during other experiments. To enable simultaneous use of the egun and laser, the egun can also be placed in an upper position to intersect the neutrals between the skimmer and the extraction region. The upper position created an electron beam parallel to the TOF axis. In this configuration, the egun made contact with only one of the acceleration plates, thus it was on at all times and did not pulse on and off. When the egun was utilized, most species are ionized under our typical operating conditions. Since species such as CH_3^+ and H^+ could be produced by dissociative electron

impact ionization of various stable molecules, other researchers[28,44] chose to carry out mass spectral measurements with low-energy electrons to minimize possible contributions from the dissociative ionization processes. In this investigation, radical measurements were carried out using a laser (REMPI) to avoid such contributions from dissociative ionization processes. REMPI measurements also may avoid isobaric interferences.

3.3.2 Laser

A laser beam was used to selectively produce ions for TOF mass spectroscopy. The UV beam employed for the REMPI measurements was produced by frequency doubling the output of a Nd:YAG-pumped pulsed dye laser (PDL) (Quantra Ray DCR2A/PDL-1) using a β-BaB_2O_4 (BBO) crystal. Two BBO crystals, one cut at $\theta = 55°$ and the other at $\theta = 40°$, were available to yield the range of wavelength from 220 - 255 nm and 255 - 340 nm, respectively. In order to improve the intensity of the doubled UV output, the Nd:YAG laser was operated in the fast pulse mode which created 2 ns pulse widths and increased peak powers. The (2+1) REMPI line through the 1s→2s transition in H lies at 243.13 nm. To obtain this excitation wavelength, LD490 dye (Exciton Chemical, Dayton, OH) was used in the PDL along with the BBO crystal (θ = 55°) producing ~ 4 mm spot size. Approximately 1.5 mJ/pulse of UV energy was produced at this wavelength. For the (2+1) REMPI line through the $X^2A_2'' \rightarrow 3p^2A_2''$ transition in CH_3 at 333.5 nm DCM dye spiked with LDS 698

dye was used in the PDL, along with the $\theta = 40°$ BBO crystal to produce a beam spot size of ~ 8 mm. The laser beam was focused in the extraction region of the chamber using a 200 mm focal length quartz lens. Back reflections of the laser beam were minimized by tilting the beam at a diagonal through the ionization region. To maintain constant laser power throughout a wavelength scan, the power was monitored at the chamber exit window and the BBO crystal was rotated manually using a motorized rotation stage.

3.4 Film Characterization

To verify that the films produced in the HFCVD chamber were diamond, scanning electron microscopy (SEM) and Raman spectroscopy were applied. Raman spectroscopy is the accepted technique for characterizing carbon bonding in diamond and diamondlike films. SEM images were used to determine surface morphology and growth rates.

3.4.1 Scanning Electron Microscopy

In 1929, Stintzing envisioned the operation of a scanning type electron microscope and in 1935, Knoll actually demonstrated this hypothesis. The first SEM was constructed by von Ardenne in 1938. SEM's did not become commercially available until the 1960's. The SEM utilizes a focused beam of high energy electrons that systematically scan across the specimen surface. The interaction of the beam with the specimen produces a variety of signals at or near the specimen surface which can be used to study the sample. These

include lower energy electrons, termed secondaries. The low energy of these secondaries allows them to be conveniently collected for SEM since they can be easily drawn to a positively biased detector system. The electron signal is eventually converted to an electronic signal which is portrayed on a cathode ray tube (essentially a television screen). The scanning beam is synchronized with the scanning of the cathode ray tube, thus producing a one-to-one relation between points on the specimen and points on the CRT. Electrons emitted from a surface which faces away from the detector are partially blocked by the specimen and the image of such a surface is darker than that of a surface which faces toward the detector.[45]

A Cambridge Leica Stereoscan 420 SEM was utilized to obtain the images presented in Chapter 4. The following settings were used to obtain images of CVD diamond: 100 μA beam current, 100 V collector bias, 20 kV acceleration voltage, and 20 pA probe current. The ultimate instrumental resolution is 5 nm.

3.4.2 Raman Spectroscopy

In Raman scattering, a electromagnetic wave inelastically scatters off a material and either loses or gains energy in units of the energy levels of the sample. The new energy differs from the incident energy by the energy of the optical photon. The intensity of scattered radiation is low, therefore very intense incident beams are required. Raman scattering is a very important tool for identifying the material and its state of stress or disorder. For diamond,

the characteristic vibrational energy is approximately 1332 cm^{-1}. Second-order Raman processes peak at 2458 cm^{-1} in natural diamond and in synthetic diamond films. Graphite peaks can exist in several locations.[46] Pure crystalline graphite can have a peak anywhere between 1580 - 1600 cm^{-1}, depending on the material preparation method. Crystalline defects cause other Raman shifts with, for example, in-plane defects in graphite causing a peak in the range of 1350 - 1370 cm^{-1} and between-plane defects indicated by a peak at 1550 - 1580 cm^{-1}.[47] Other peaks have not been unambiguously identified, but are thought to be due to defects in sp^2 bonded carbon. The peak positions depend on the size of the graphite crystallites. The Raman effect is approximately 100 times more sensitive to graphite bonding than to diamond (depending on the wavelength of the exciting radiation).[48] Thus, small amounts of graphite can be easily detected. Raman spectra for natural diamond, graphite, diamondlike carbon, and diamond film are shown in Figure 3.4.[49] The differences in these spectra illustrate the utility of Raman spectroscopy in determining carbon bonding in diamond films.

A Dilor XY Modular Laser Raman Spectrometer from EG&G was employed to obtain the Raman spectra in Chapter 4. The spectrometer consists of a double foremonochromator coupled to a spectrograph with a charged coupled device (CCD) detector. The excitation was accomplished using a Lexel 350 Ar ion laser operated at 514.5 nm with 100 mW power. The Dilor triple monochromator was run in the subtractive mode with a 100 μm slit, producing a bandpass of 4.72 cm^{-1}. The spectrometer contains provisions for macro and

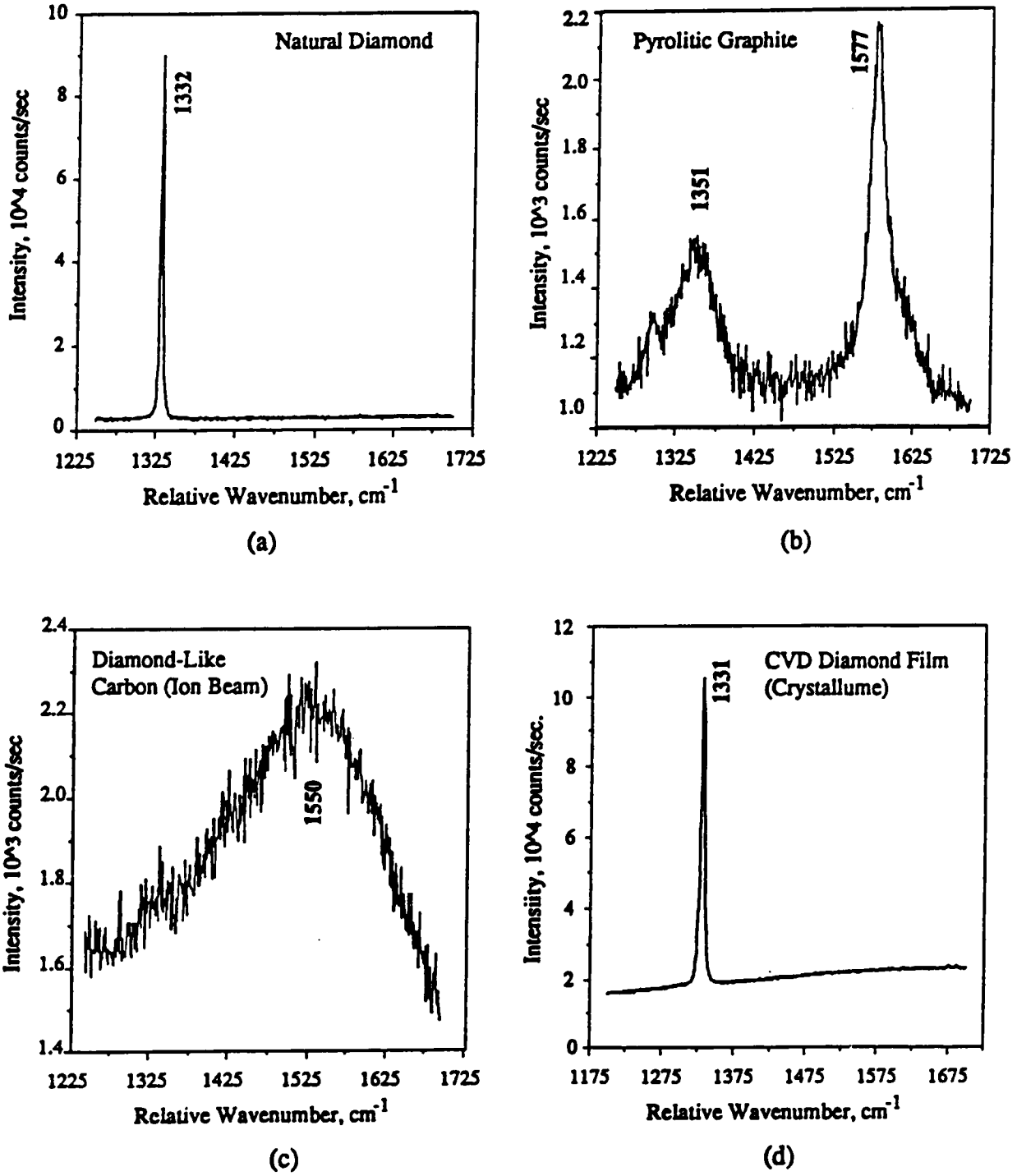


Figure 3.4 Raman spectra for (a) natural diamond, (b) highly oriented pyrolytic graphite (HOPG), (c) diamondlike carbon, and (d) diamond film.

micro sampling. All spectra in this thesis were recorded on a microscope stage with a 100X objective with integration times of 50 s. A confocal aperture limited the spatial sampling to ~ 8 μm. The CCD detector was thermo-electrically cooled to -70 °C.

3.5 Summary

The HFCVD reactor with TOF mass spectrometer described in this chapter was utilized for all the experiments discussed in this thesis. Reactor conditions were repeatable from day to day. The Raman measurements were performed at The University of Tennessee while the SEM images were obtained at Oak Ridge National Laboratory.

In the following chapter, the effects of filament and substrate temperature on the composition of the gases present immediately above the diamond growth surface are presented. Correlations between these results and diamond film growth are discussed.

Chapter 4

Results and Discussion

4.1 Introduction

The concentrations of the major stable and radical species present in the reactor were monitored using EI or REMPI mass spectrometry as a function of substrate and filament temperature. All results were obtained with an initial gas composition of 0.5% CH_4 and 1% each of He, Ne, and Ar in H_2 with a total flow of 100 sccm, unless otherwise stated. Typical pressures were 80 Torr in the growth region, 1 x 10^{-3} Torr in the expansion region, and 2 x 10^{-6} Torr in the mass spectrometer. When measuring CH_4, data was acquired for m/z=15 and m/z=16 to verify that the signal at m/z=16 was CH_4 and not O. The intensities at m/z=15 and m/z=16 tracked each other well indicating little to no O was present. After each change in temperature (filament and/or substrate), a minimum of 30 minutes passed allowing the system to equilibrate before mass spectral scans were collected. Data points have approximately a 7 to 10% error resulting from the precision of the signal peak heights. A minimum of 3 scans were averaged for each data point. For EI measurements, baselines were determined by an average of points before and after the mass peak of interest. For the REMPI measurements, baselines were determined at an off resonance wavelength.

4.2 Electron Impact Ionization

From the results, the chemical dependence on the substrate and filament temperatures must be extracted. A complication arises from the physical variations of the signal strength due to the change in the source number density with T. In an effusive flow on axis, the number density will be proportional to the source number density and both EI and REMPI signals should have a T^{-1} dependence. For molecular flow, there is not a direct proportionality between the number density and the source number density due to a focusing of the beam. The signals have a T^{-m} dependence with $m > 1.5$[0] The Ne signal as a function of substrate temperature is compared to a T^{-1} temperature dependence in Figure 4.1. This illustrates the effect due to the change in gas density with temperature. Since the noble gases are non-reactive, they can be utilized for normalization purposes.

To normalize, the data presented was divided by the intensity of a noble gas peak obtained under identical operating conditions. The noble gas chosen for the normalization procedure was determined by a similarity in mass/charge (m/z) or signal intensity. Figure 4.2 illustrates how normalization can correct for physical changes occurring in the system. Figure 4.2 (a) shows the uncorrected EI ionization intensities for m/z = 15, 16, 26 as a function of substrate temperature (T_s) at fixed filament temperature, T_f = 1890 °C. There is a discontinuity at T_s > 800 °C. When the data was normalized to $_{40}Ar^{2+}$ (Figure 4.2 (b)), the discontinuity disappears. Following an adjustment in the

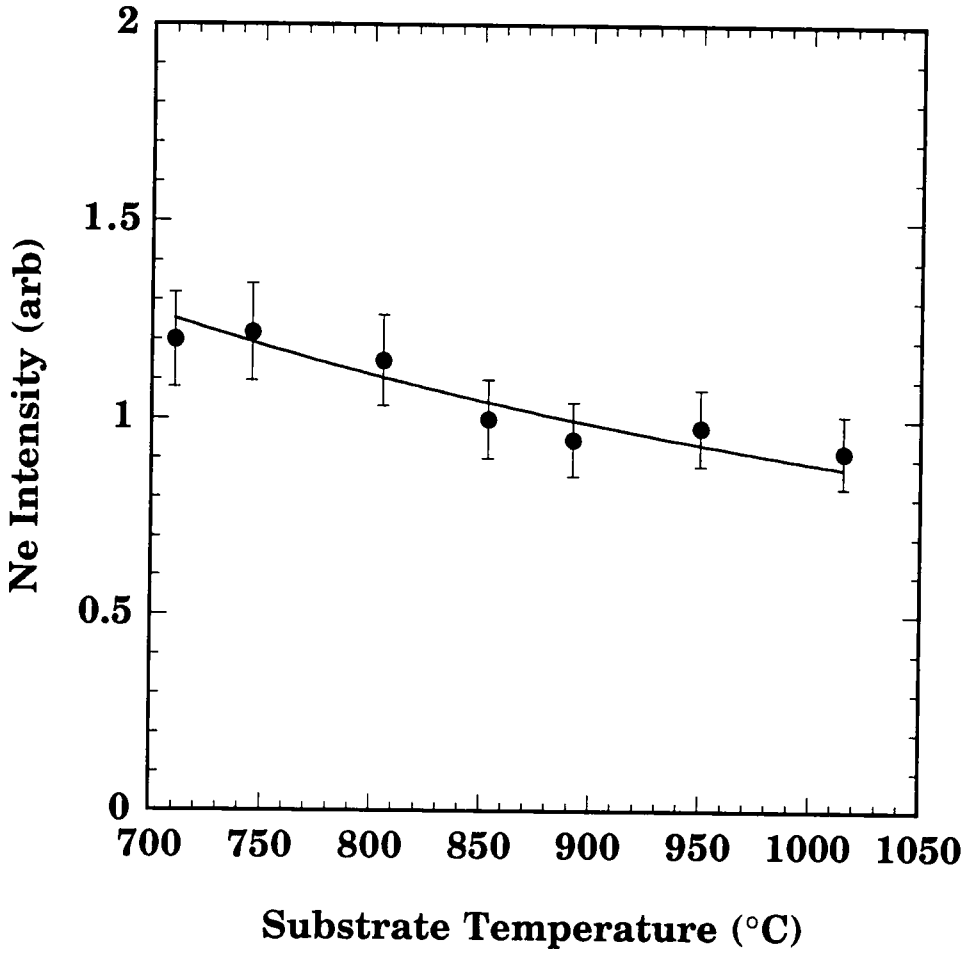


Figure 4.1 Dependence of the Ne EI signal on substrate temperature. Curve shows a fit to a T^{-1} variation expected due to an ideal gas expansion.

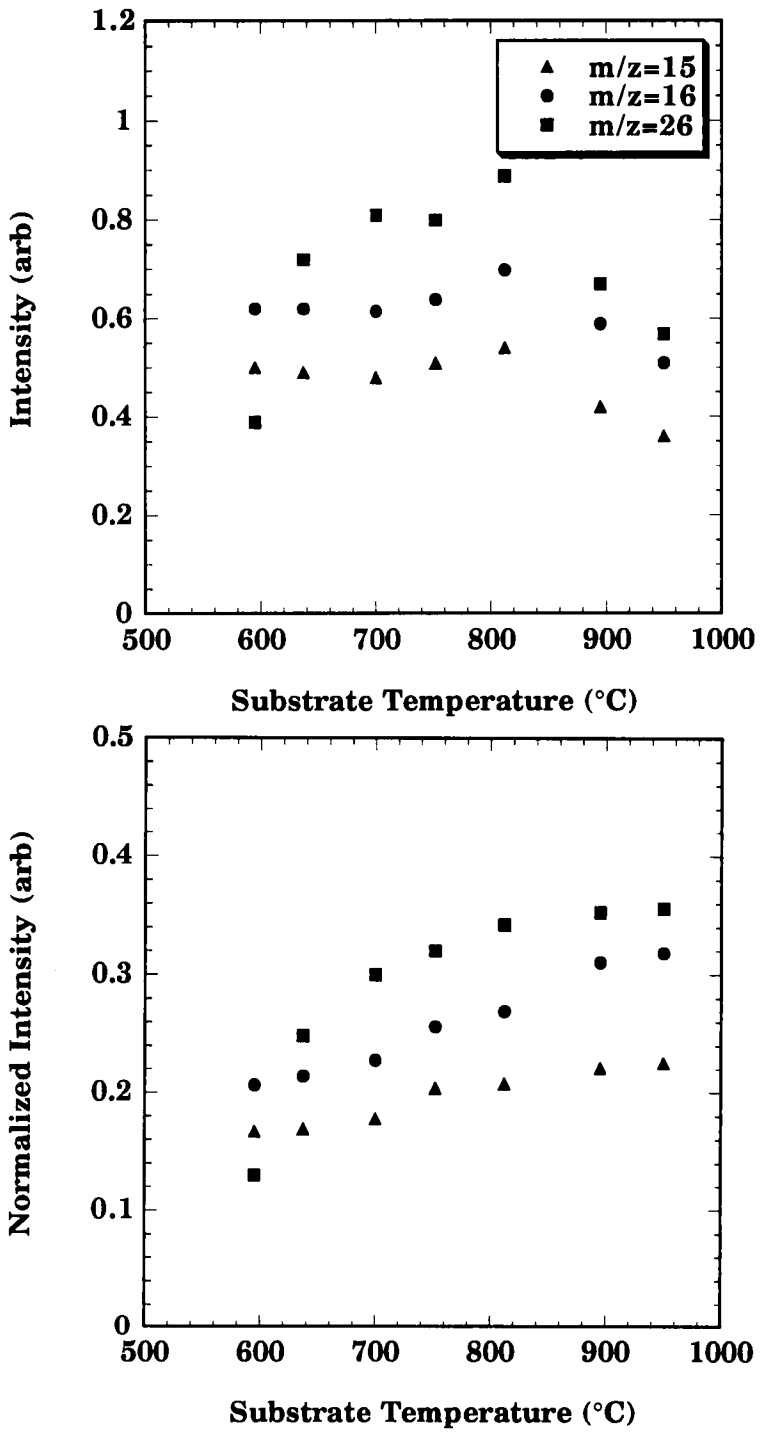


Figure 4.2 a) Raw data for varying T_s with T_f = 1890 °C. b) Normalized data to m/z = 20.

wiring, the experiment was repeated to determine if the break point was a mechanical problem or change in beam character. The new data did not contain a discontinuity, yet produced similar normalized results. Thus normalizing the data not only eases identification of changes in gas composition due to changes in temperature in the reactor but can eliminate effects of mechanical failures of the system as well.

To characterize the flow in the system, 5% He, Ne, and Ar in H_2 was metered into the chamber at a constant rate of 100 sccm. Figure 4.3 shows intensity measurements as a function of T_s. The He and Ar signals were normalized to ^{22}Ne, a 9% abundance isotope, to avoid confusion due to doubly ionized Ar at m/z = 20. Differences in ionization cross sections (He: 0.34×10^{-20} m^2, Ne: 0.57×10^{-20} m^2, Ar: 3×10^{-20} m^2)[51, 52] were taken into account in the results. When mass focusing within the sampled beam does not occur, substrate temperature variations should have little effect on signal intensity, resulting in a uniform normalized signal intensity with changing T_s. This was observed at $T_s > 400$ °C for both He and Ar; therefore, the system does not experience mass discrimination under typical diamond growth conditions. Room temperature results (Figure 4.3) indicate that the beam is mass focused. For the room temperature measurements, the filament was off. The Ar signal (Figure 4.3 (b)) was larger at room temperature than at elevated temperatures, indicating that the larger masses were focused in the center of the beam. The He signal (Figure 4.3 (a)) was smaller at room temperature

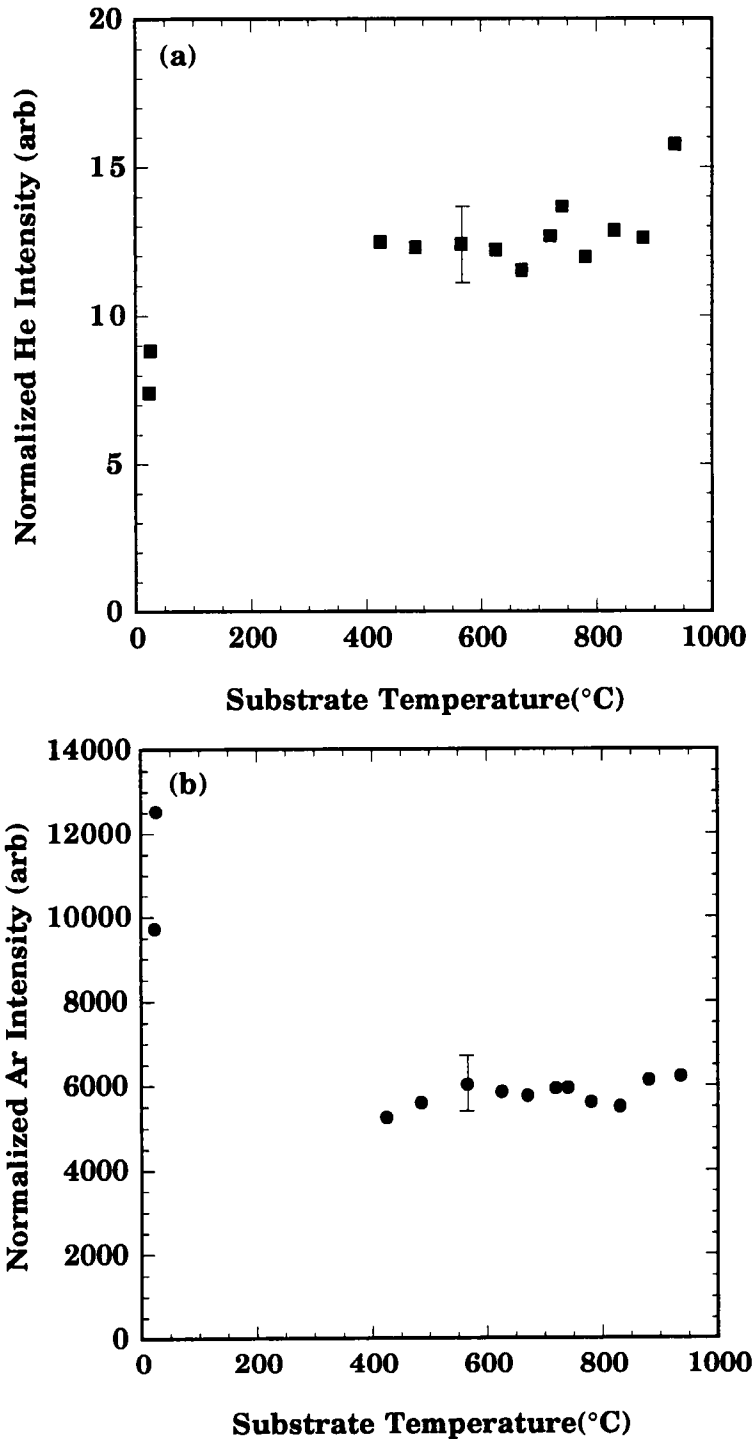


Figure 4.3 Substrate temperature dependence of (a) He and (b) Ar signals, normalized to Ne (m/z = 22).

than at higher T_s, resulting from its lower mass not being focused as tightly. These results indicate that the system has effusive flow under growth conditions and molecular flow at lower temperatures. Calculations regarding beam characterization and ion count are located the Appendix.

Electron impact ionization results for CH_4 decomposition and C_2H_2 production with varying filament temperature are shown in Figure 4.4. Films were deposited for 18 hours at the three indicated conditions labeled A, B, and C (discussed in §4.4). All measurements were performed with the substrate temperature fixed at 780 °C. The conversion of CH_4 to C_2H_2 reached a midpoint at T_f = 1700 °C. Only minor differences were obtained when the substrate temperature was allowed to vary with changing filament temperature. Corat and Goodwin reported a similar finding at 1800°C when sampling stable gases near the substrate through a capillary probe.[53] The difference in emissivity of Re and C coated W filaments accounts for the deviation in the midpoint temperatures. Sommer and Smith have argued that the sharp change in gas composition as the filament temperature increases results from filament poisoning at low temperatures, due to a graphite layer coating the filament.[54] For 0.5% CH_4 in H_2, the carbon-hydrogen equilibrium phase diagram shows that graphite is stable below about 1900 °C. These results (Figure 4.4) are consistent with this interpretation. Once the graphite layer desorbs, the CH_4 and C_2H_2 signals saturate and are unaffected by further increases in filament temperature.

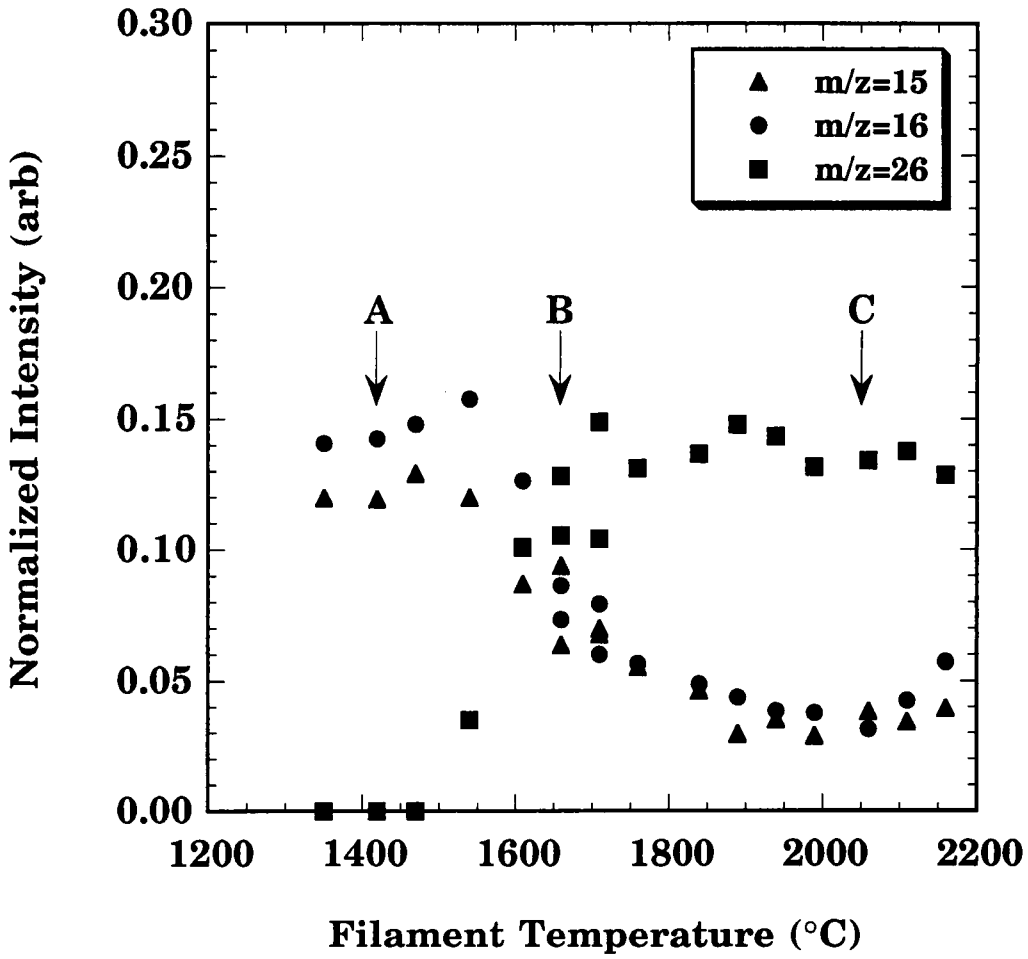


Figure 4.4 Electron impact ionization of methane and acetylene verses filament temperature with T_s = 780 °C. Films were grown at A, B, and C.

Figure 4.5 (a) shows that the relative CH_4 concentration was independent of substrate temperature with T_f = 1890 °C. The C_2H_2 signal rises and then appears to plateau, indicating that substrate temperature can influence gas phase concentrations. At T_f = 1420 °C (Figure 4.5 (b)), the results for CH_4 are similar with no apparent effect of T_s. The C_2H_2 intensity decreased with increasing T_s, indicating its possible incorporation into the diamond film at low filament temperatures. M/z = 20 was used for normalization in Figure 4.5.

4.3 Resonance Enhanced Multiphoton Ionization

Several options were attempted for the normalization of the REMPI data. First, a (2+2) REMPI of He was tried at 240.57 nm for the transition $1s^2\ 1S_0 \rightarrow 2s^2\ 2S_0$ because it was in the same dye range as a H (2 + 1) REMPI transition. The signal was not intense enough to be utilized without introducing large errors into the results. The (3 +1) REMPI signal at 314.4 nm from the Ar $3p^6\ {}^1S \rightarrow 3p^5 4s4s'\ [1/2]^\circ\ J=1$ transition was also tested. Since the 4s′ transition is dipole-allowed, retroreflection of the beam to form a standing wave geometry is necessary to avoid cancellation of the REMPI signal by competing third harmonic generation.[55] The signal is extremely sensitive to the precise overlap of the beams at the focus which proved to be an extremely difficult setup. EI measurements were also attempted with the egun in the upper position. In the upper position, the quartz windows were still in place allowing REMPI and EI measurements to be taken concurrently. The egun did not

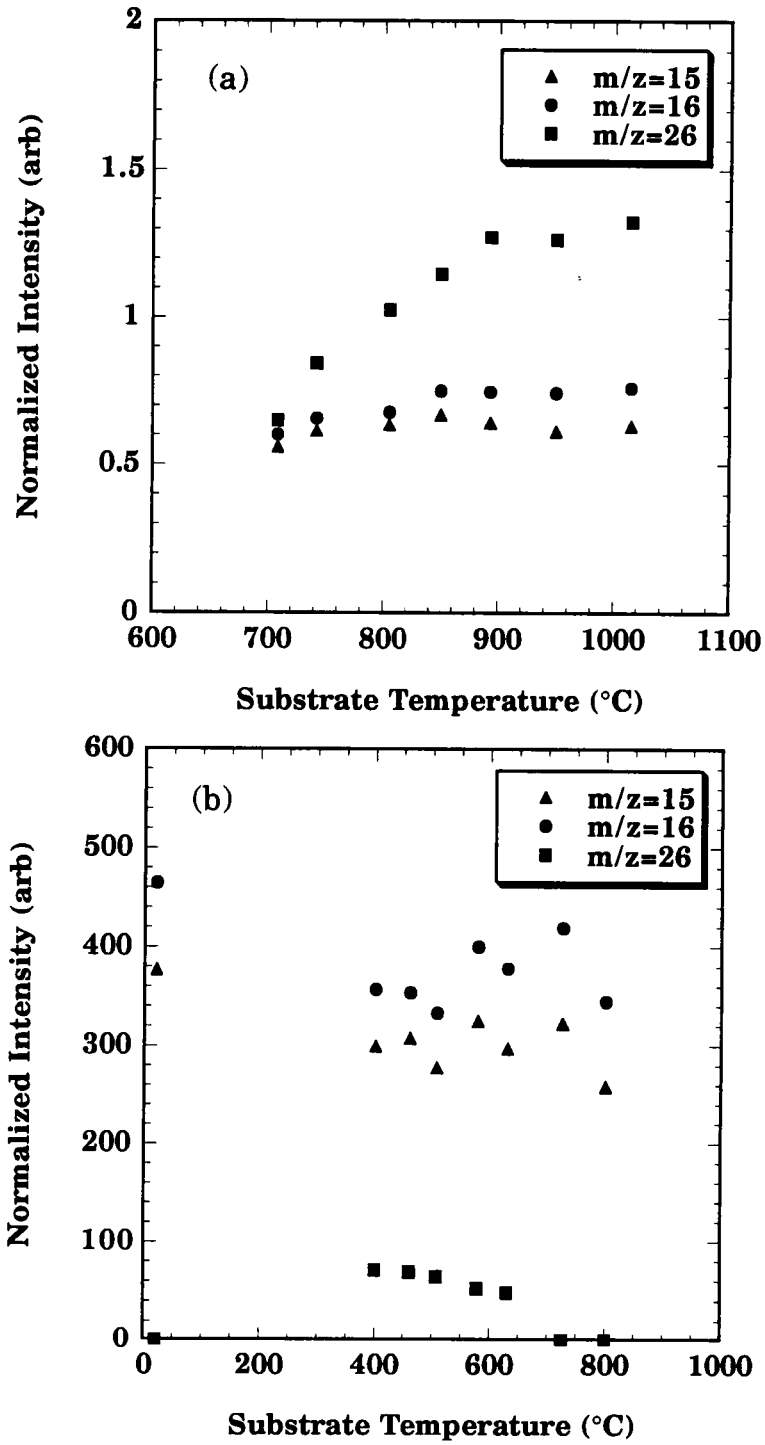


Figure 4.5 Substrate temperature dependence of methane and acetylene with (a) T_f = 1890 °C and (b) T_f = 1420 °C, normalized to m/z = 20.

provide ample signal intensity in the upper position due to a flaw in the design. EI in the lower position was resorted to for normalization. REMPI data was collected and then the conditions were repeated with the egun in the lower position to collect data for normalization. The conditions in the chamber were repeatable from day to day. All data used for normalization was taken with the same hot filament. H and CH_3 REMPI intensities were obtained by taking wavelength scans to obtain peak intensity and baseline information. An average of at least three scans is presented at each temperature.

4.3.1 Atomic Hydrogen

Atomic hydrogen was detected using a (2+1) REMPI technique in which two 243.13 nm photons were absorbed simultaneously to excite the (1s $\rightarrow$ 2s) Lyman-α transition and a third photon of the same wavelength caused the subsequent ionization from the 2s level. Figure 4.6 shows the energy level diagram for H.[56] Figure 4.7 illustrates the wavelength dependence of the H (2+1) REMPI signal.

The dependence of the H REMPI signal on the filament temperature is shown in Figure 4.8. T_s was fixed at 730 °C. The peak intensity of the resonant 243.13 nm multiphoton ionization feature increased with increasing filament temperature. H did not appear to reach a maximum value under typical diamond growth conditions as did other species (i.e. CH_4 and C_2H_2). There is an exponential dependence of the H REMPI signal on T_f, and is therefore

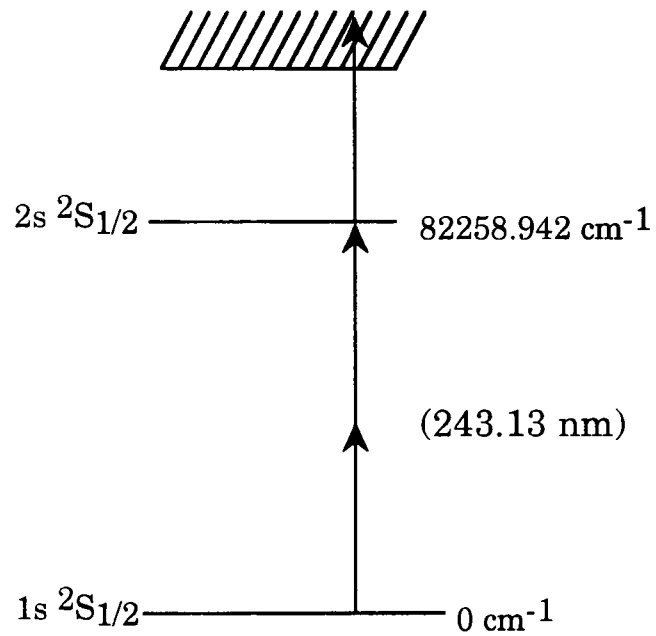


Figure 4.6 Energy level diagram for atomic hydrogen illustrating the (2+1) REMPI transition observed in this work.

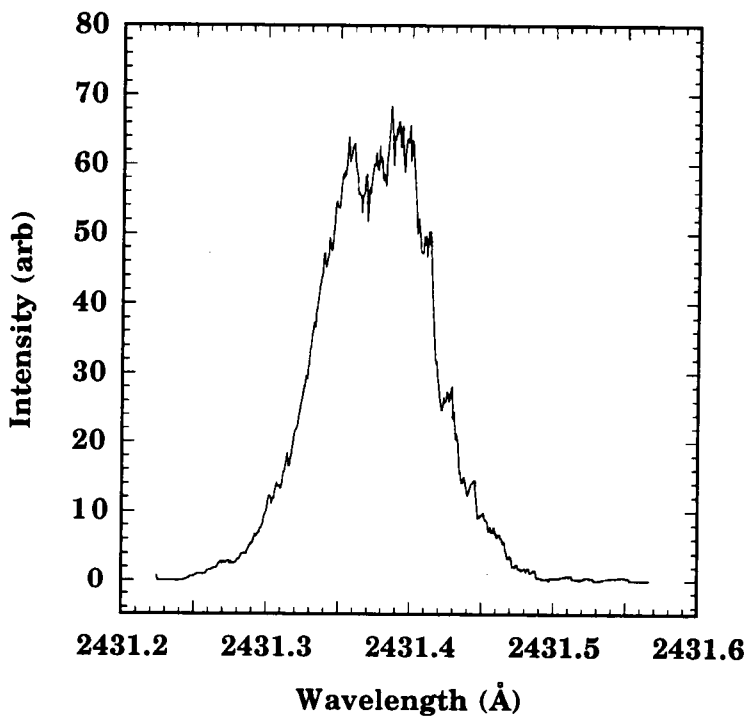


Figure 4.7 Wavelength dependence of the H (2+1) REMPI signal at 234.13 nm.

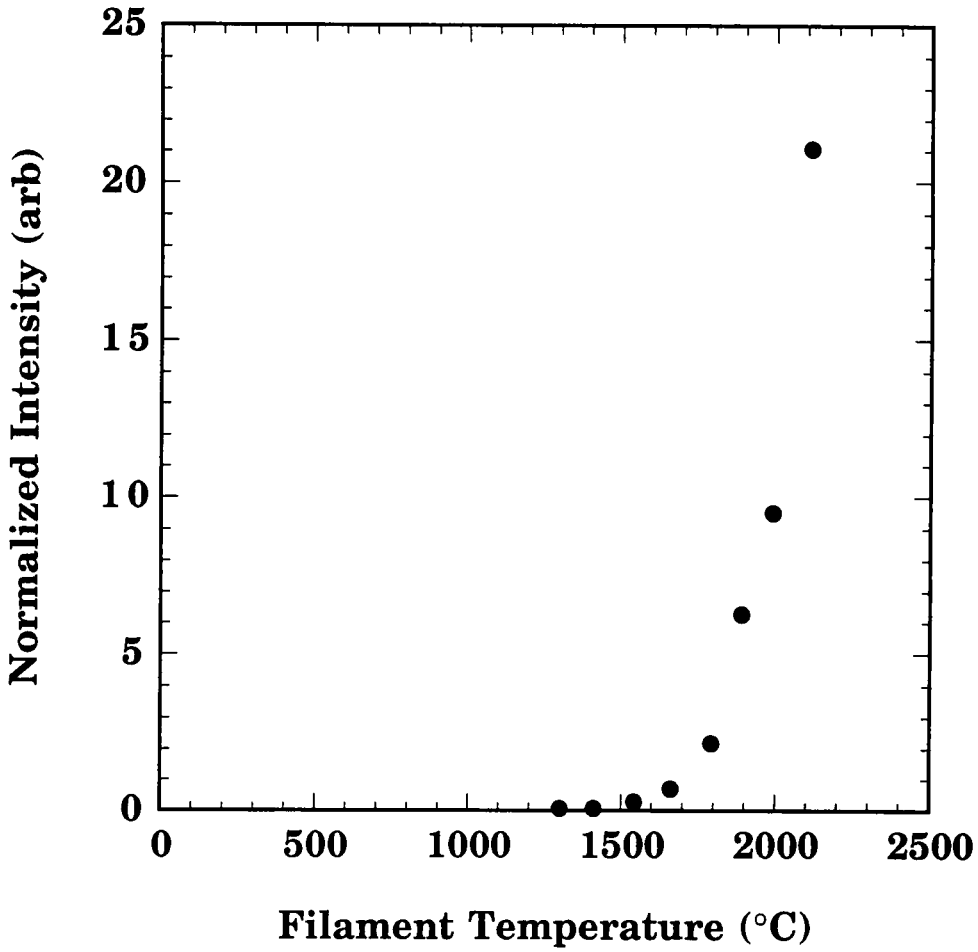


Figure 4.8 Dependence of H REMPI signal on filament temperature with T_s = 730 °C.

consistent with the Boltzmann constant ($k \propto e^{-E_a/kT}$). Celii and Butler reported similar results utilizing a (3 + 1) REMPI with 364.7 nm photons for the ($1s \rightarrow 2p$) transition.[40] Figure 4.9 shows that the relative H concentration decreased with increasing substrate temperature. T_f was fixed at 1890 °C. Both Figure 4.8 and 4.9 were normalized to Ar (m/z = 40).

These measurements did not specify the role of H in the mechanism for diamond deposition. H is a highly reactive species and is believed to be one of the most important in the gas phase and on the surface for CVD diamond growth. H is created at the hot filament through the dissociation of H_2. At the surface, H is believed to maintain a hydrogen-terminated diamond surface and abstracts surface hydrogens to form reactive radical sites for diamond growth. Its presence on the surface precludes the growth of graphite[57] and perhaps also preferentially reacts with any graphite carbon that is formed.[58, 59]

4.3.2 Methyl Radical

Hudgens et al. investigated the two photon REMPI spectroscopy and state assignments of CH_3.[60] Molecular orbital calculations predict a planar D_{3h} structure with no barrier to inversion. In D_{3h} symmetry, the ground state of CH_3 has the electron configuration,

$$(1a_1')^2(2a_1')^2(2e')^4(2a_2'')^1, X\ ^2A_2'',$$

and $^2A_2''$ symmetry.

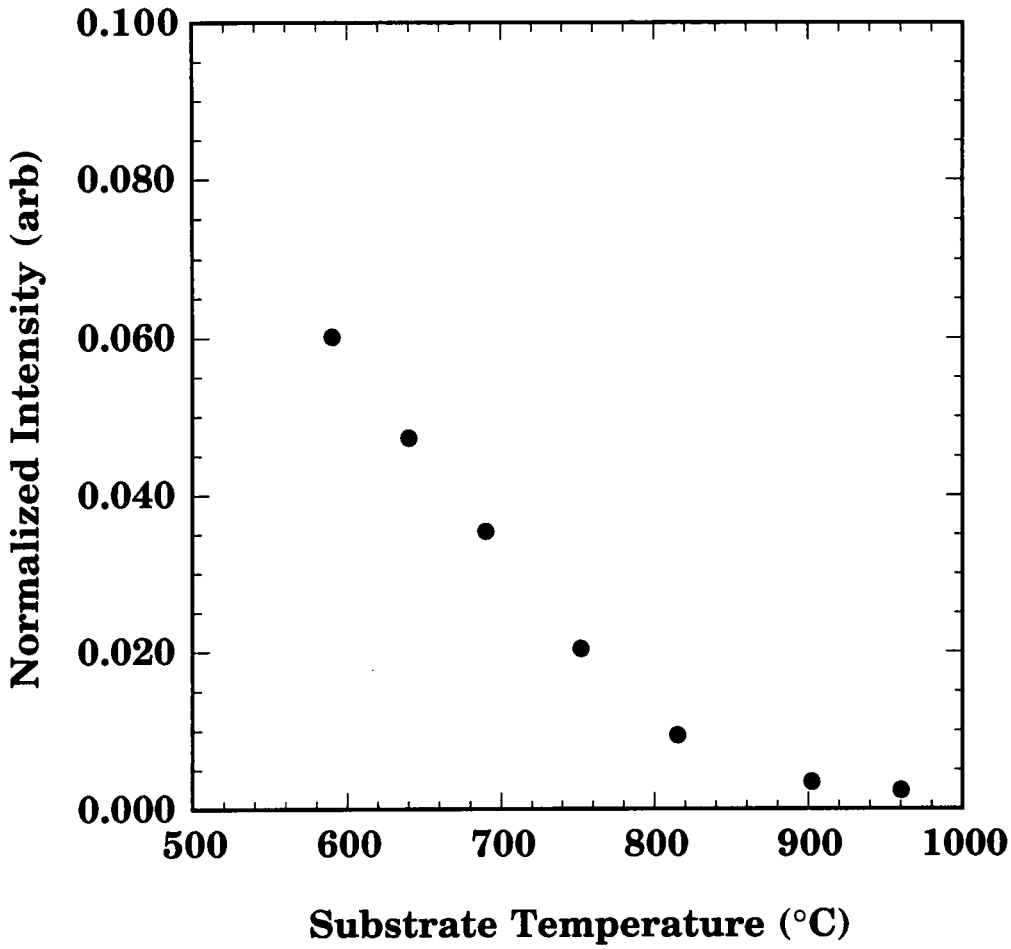


Figure 4.9 Dependence of H REMPI signal on substrate temperature with T_f = 1890 °C.

An energy level diagram for CH_3 is shown in Figure 4.10. The CH_3 REMPI peak at 333.5 nm results from the vibrationless (0-0) two photon absorption from the $X\ ^2A_2''$ electronic ground state to the $3p^2A_2''$ vibrationless state followed by single photon ionization. Figure 4.11 illustrates a wavelength verses CH_3 signal intensity scan. The observed peak is the strong Q branch of the band, whose rotational structure is completely unresolved. Figure 4.12 presents mass spectra obtained with the laser tuned on and off the resonance wavelength for CH_3. The intensities have been offset in order to present both spectra in the same figure.

The dependence of the CH_3 REMPI signal on filament temperature is plotted in Figure 4.13. The CH_3 signal increased with increasing T_f, as expected. Celii and Butler observed a plateau or decrease in the CH_3 intensity above the substrate with filament temperatures above 2200 °C for CH_4/H_2 concentrations of 0.5, 1.0, and 2.0%.[61] There appears to be a similar result in Figure 4.13 for the last data point. The data was not extended to higher T_f values because it was not possible to maintain T_s = 730 °C with higher filament temperatures. Figure 4.13 was normalized to Ar (m/z = 40).

The dependence of CH_3 REMPI signal on the substrate temperature is depicted in Figure 4.14. The CH_3 concentration rose as T_s was increased from 700 °C to 850 °C, then decreased and flattened with higher T_s. Corat and

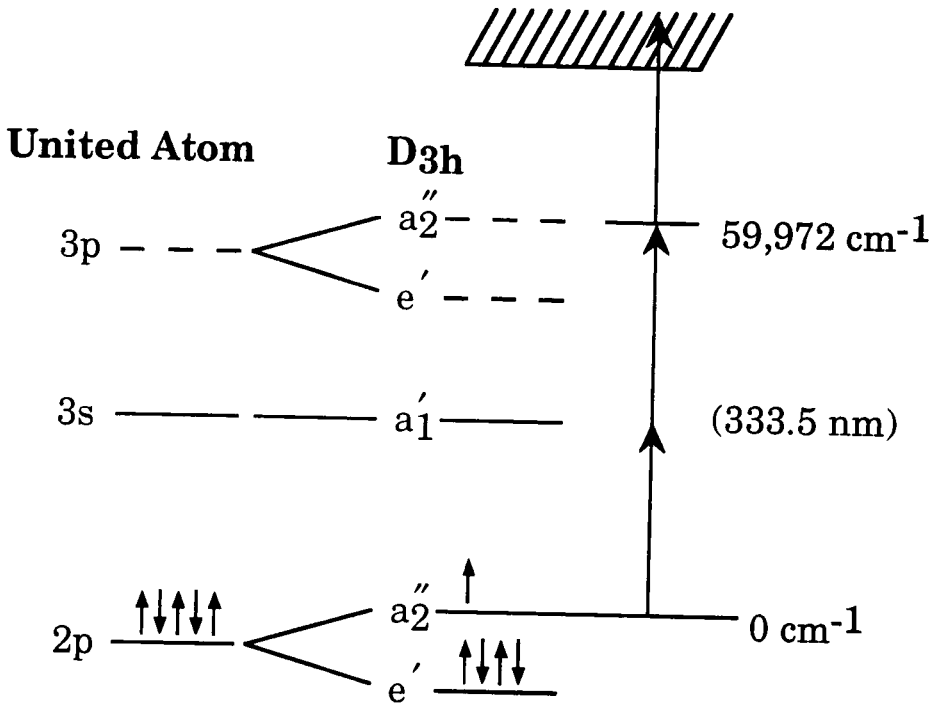


Figure 4.10 Correlation diagram between united atom, fluorine, and the D_{3h} symmetry orbitals of methyl radical. Arrows indicate the two photon transition observed in this work.

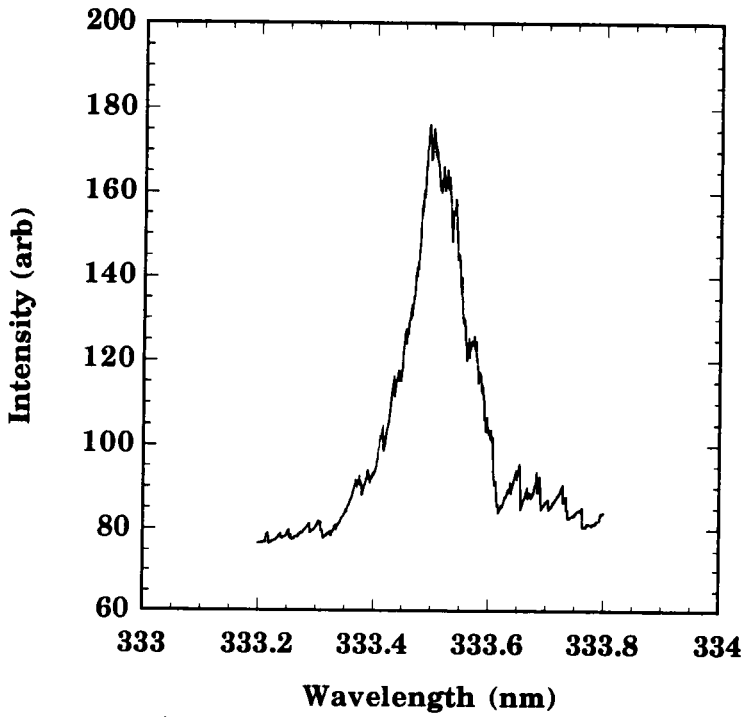


Figure 4.11 The (2+1) REMPI signal of CH_3.

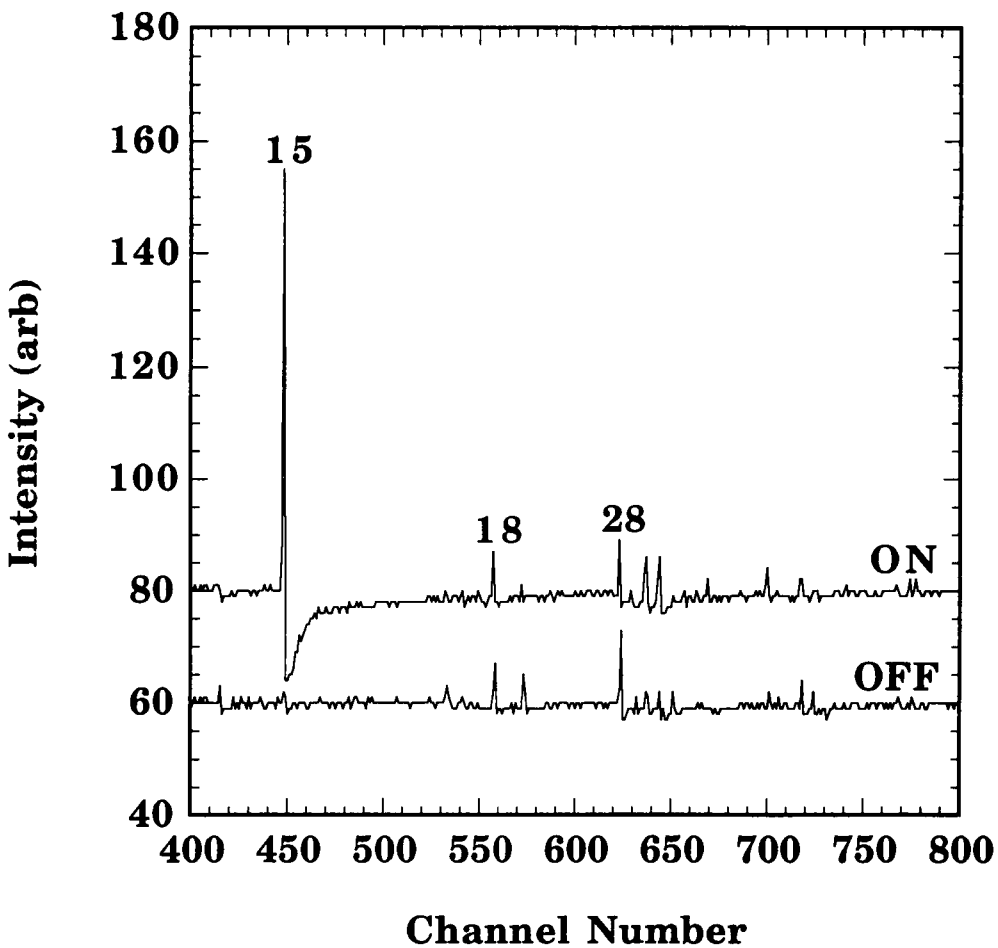


Figure 4.12 Mass spectra of expansion gases under diamond growth conditions with laser tuned on and off the (2+1) REMPI wavelength for CH_3.

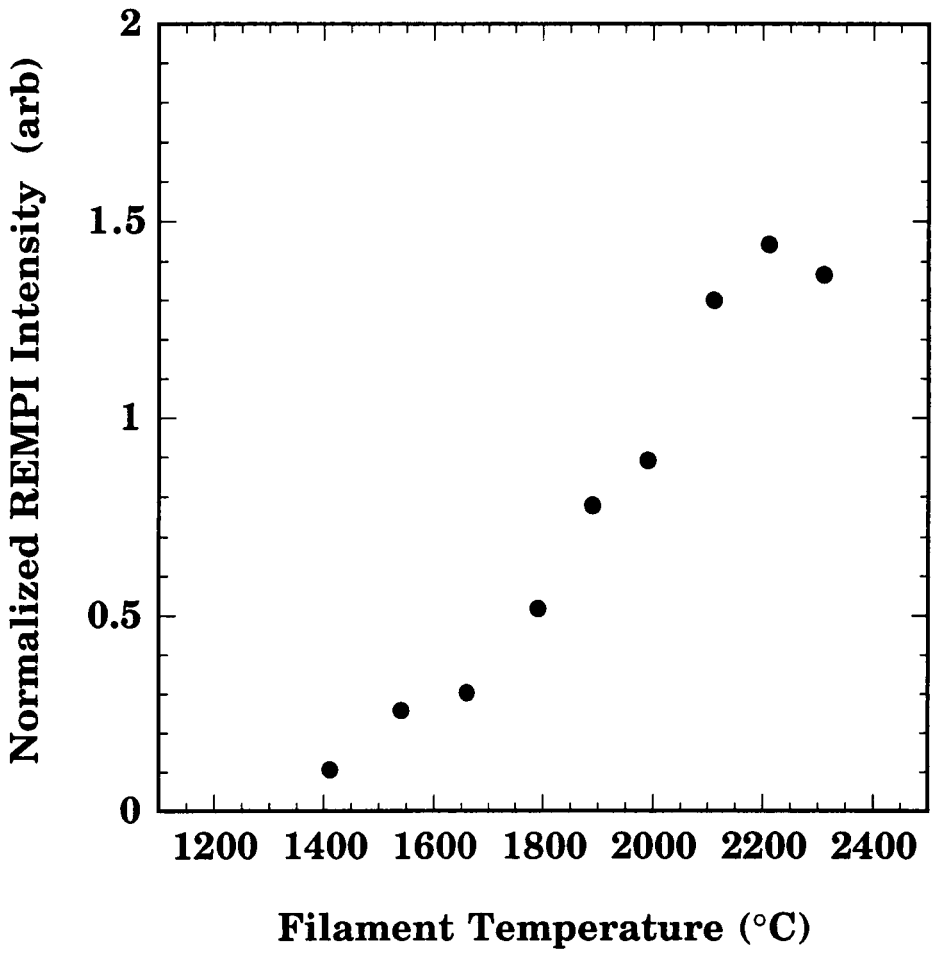


Figure 4.13 Dependence of the CH_3 signal on filament temperature with T_s = 730 °C.

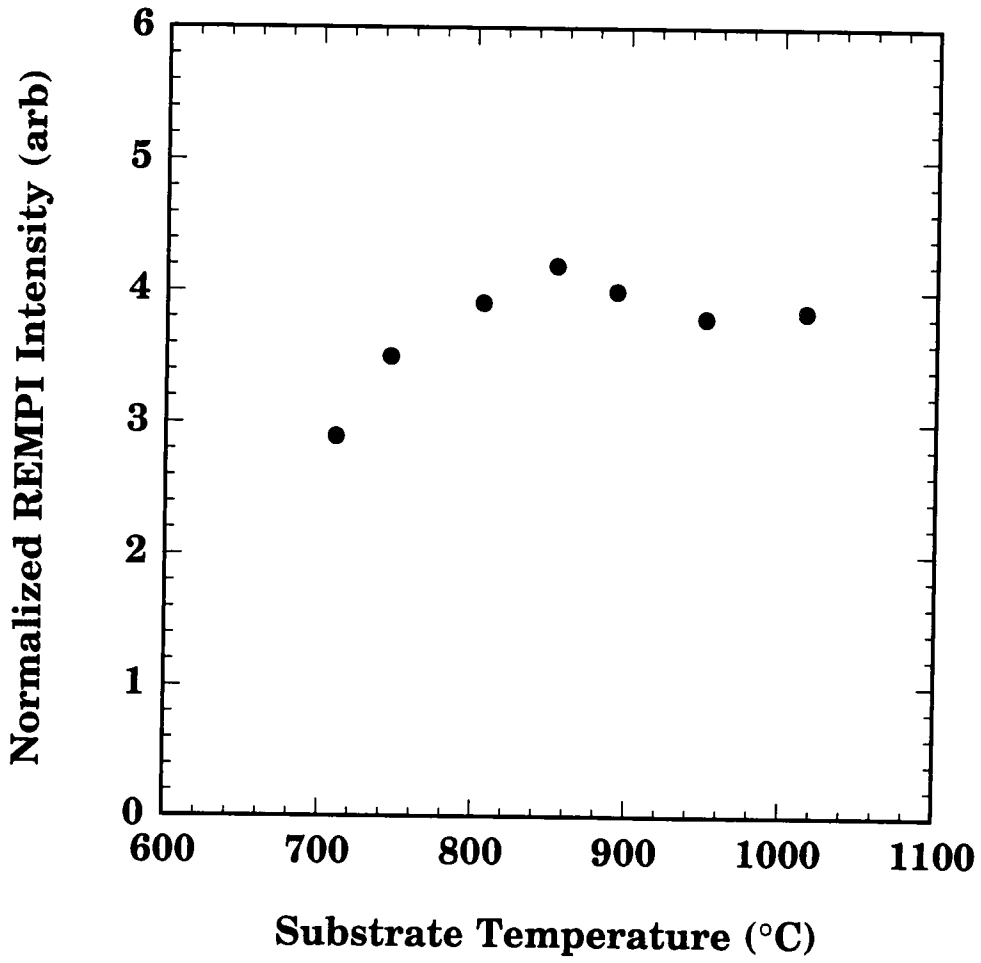


Figure 4.14 Dependence of the CH_3 signal on substrate temperature with T_f = 1890 °C.

Goodwin observed similar results with a laser beam that was focused above a substrate. They also observed that the CH_3 intensity decreased at $T_s < 700$ °C.[53]

These measurements are the first spectroscopic detection of CH_3 using orifice sampling. Corat and Goodwin[53] and Celii and Butler[61] sampled bulk reactor gases.

4.4 Film Growth

CVD diamond morphology is often discussed in terms of growth rate ratios and α values. Both Clausing et al. and Wild et al. have described how the relative growth velocities (υ) in the <100> and <111> directions determine crystal shape and film texture.[62-64] Figure 4.15 illustrates the (100), (110), and (111) planes of the diamond lattice. Figure 4.16 presents a simple picture that is helpful in the determination of grow rate ratios and therefore α values. The parameter α is defined as $\alpha = (\upsilon_{100}/\upsilon_{111})\sqrt{3}$. For large α (near 3), <100> growth is the fastest, isolated crystals are nearly octahedral with only small {100} faces and films have a <100> texture. For small α (near 1), <111> growth is the fastest, isolated crystals are nearly cubic with small triangular facets and films develop a <111> texture. For α = 3/2, isolated crystals are cubo-octahedral and <110> film texture is favored.

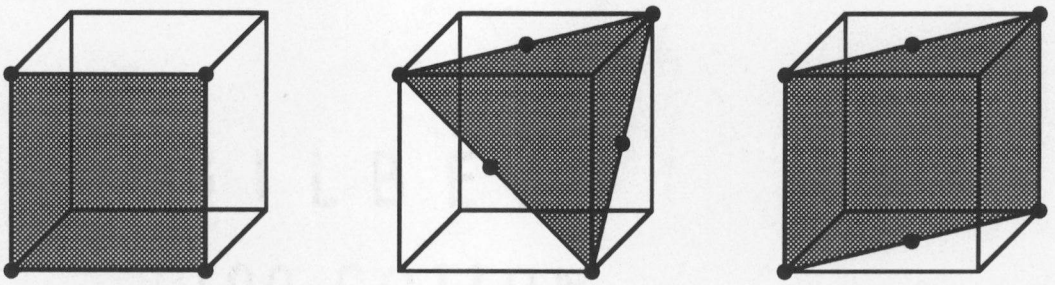


Figure 4.15 Face centered cubes illustrate the (100), (111), and (110) faces.

Table 4.1 summarizes the growth conditions and resulting α values for films deposited from 0.5% CH_4/H_2 for 18 hours. Figure 4.17 a) to d) are SEM images of isolated diamond crystals and correspond to the labels in Table 4.1. It is apparent that as the filament temperature increased, the α parameter decreased. When the filament temperature is constant, lower substrate temperatures produce crystals with higher α values.

Table 4.1 Diamond film growth conditions and resulting α values.

Film Label	T_s (°C)	T_f (°C)	$\upsilon_{100}/\upsilon_{111}$	α
A	780	1420	>1.5	>2.6
B	780	1670	0.8	1.39
C	780	2110	0.6	1.04
D	515	1670	1.5	2.6

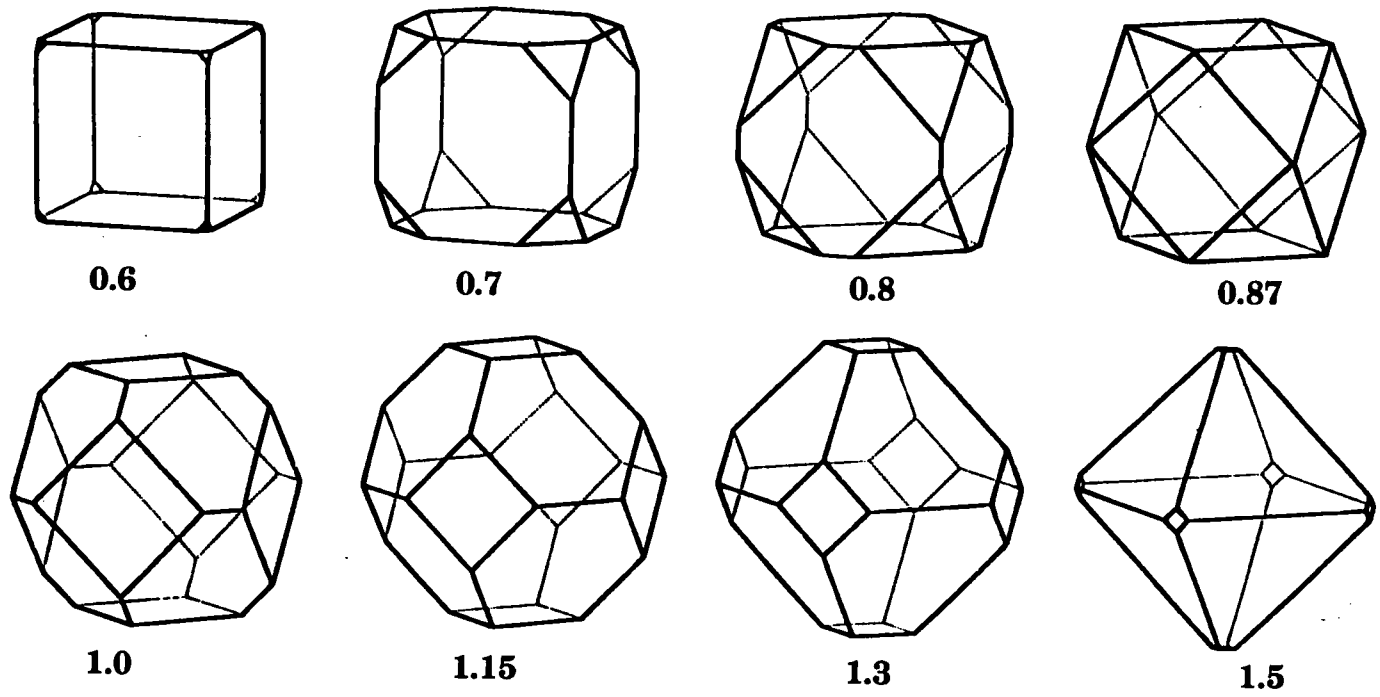
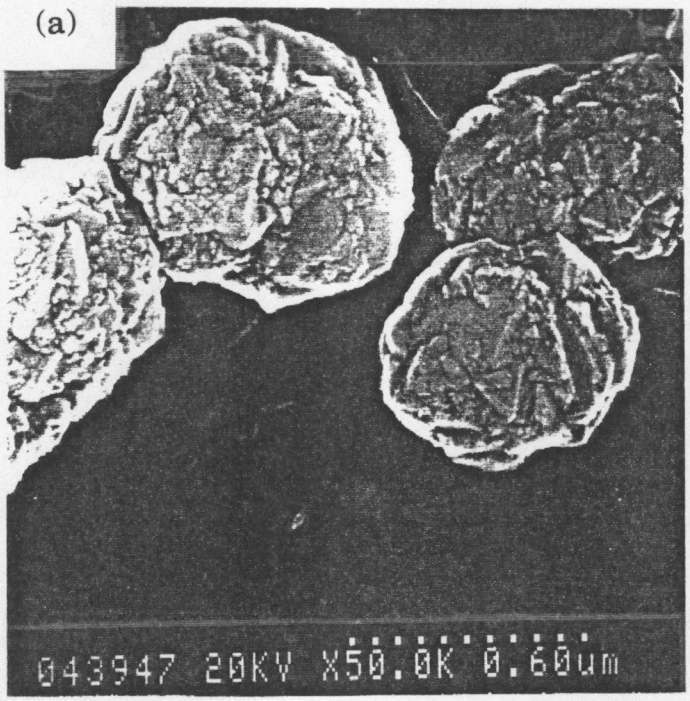


Figure 4.16 Cubo-octahedral shapes reveal the growth rate ratios on the<100> and <111> axes. The v_{100} / v_{111} is given below each shape.



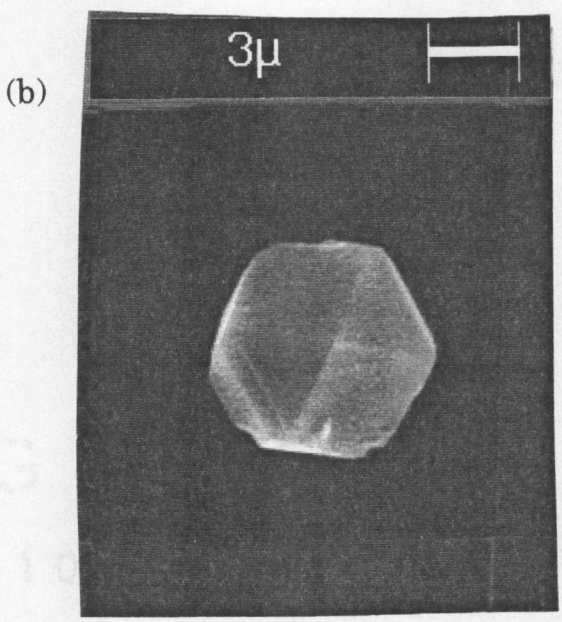
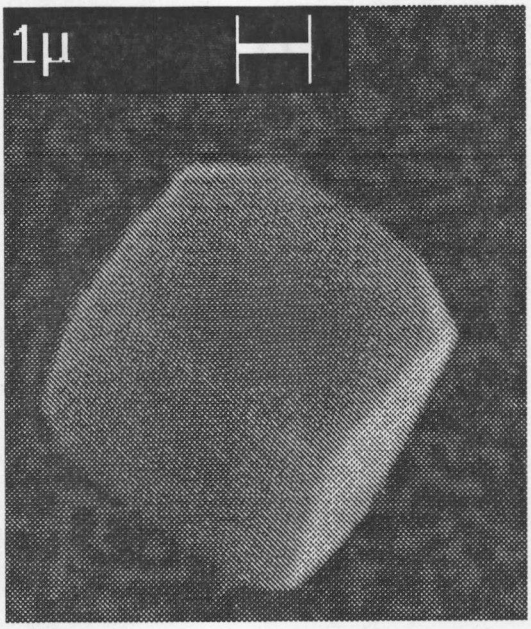


Figure 4.17 SEM images of single crystals. (a) T_f = 1420 °C, T_s = 780 °C; (b) T_f = 1670 °C, T_s = 780 °C (continued on next page).

(c)



(d)

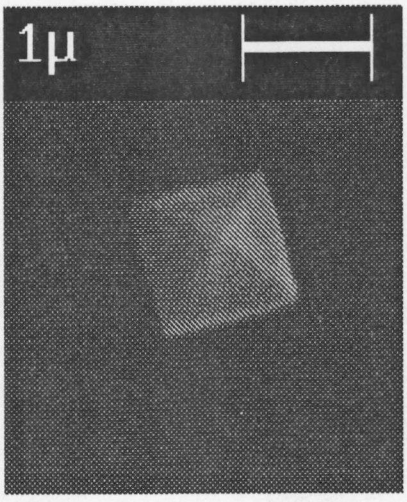


Figure 4.17 (continued) SEM images of single crystals. (c) T_f = 2110 °C, T_s = 780 °C; (d) T_f = 1670 °C, T_s =515 °C.

Raman spectra were also taken on the 4 CVD films and are presented in Figure 4.18. Film A produced a diamond peak, a weak graphite peak, and a strong Si peak indicating that diamond was produced at a slow rate. Film B exhibited a small Si signal indicating the development of a continuous film. There is a large luminescence background, diamond and graphite signals. Film C produced a strong, sharp diamond line with little to no shift relative to a natural diamond sample. There was no Si signal and no graphitic background. The sharpness of the diamond peak and low graphitic background indicate that it is an extremely high quality film. Film D exhibited an intense diamond peak, a graphite peak and a Si peak.

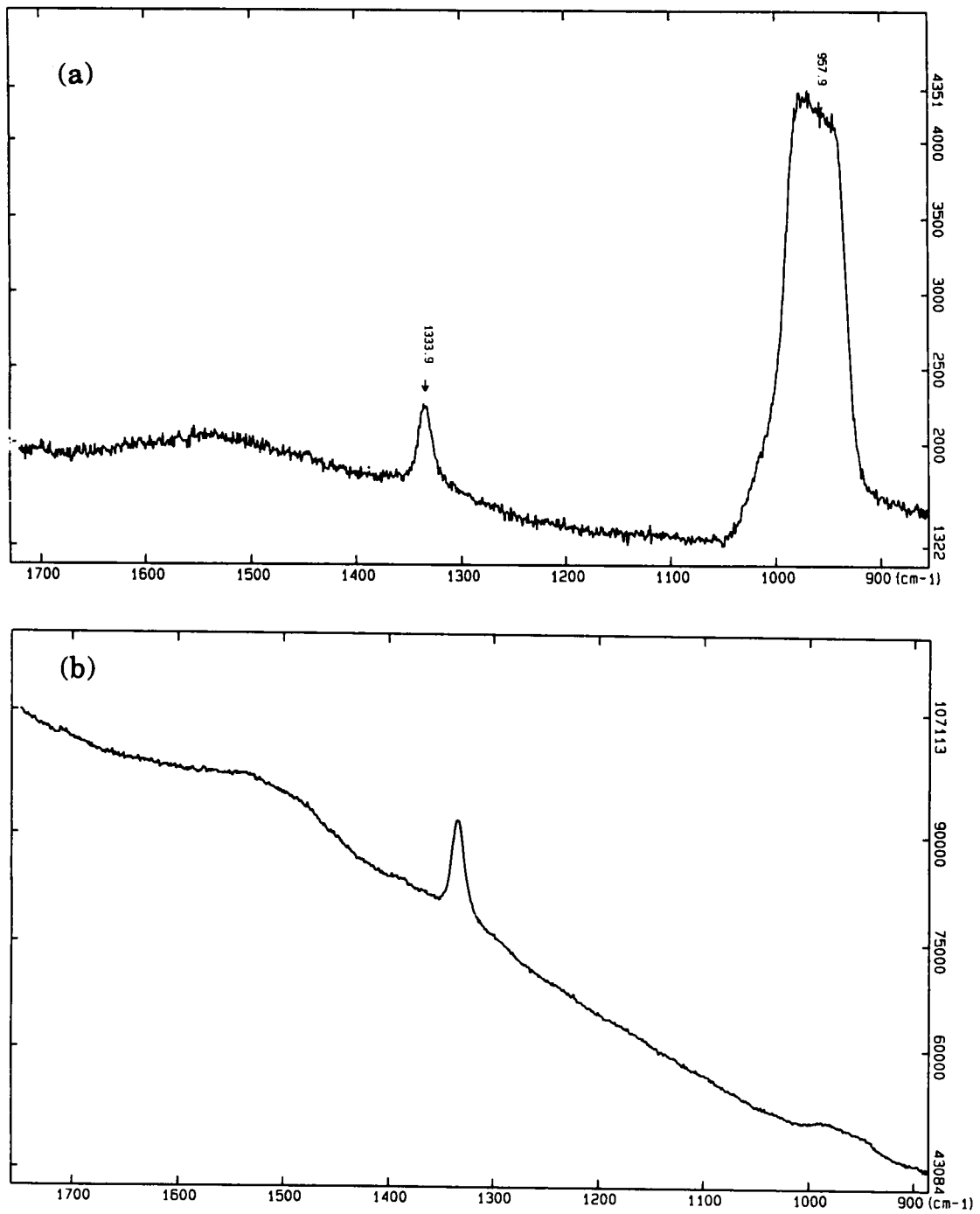


Figure 4.18 Raman spectra of CVD films. (a) T_f = 1420 °C, T_s = 780 °C; (b) T_f = 1670 °C, T_s = 780 °C (continued on next page).

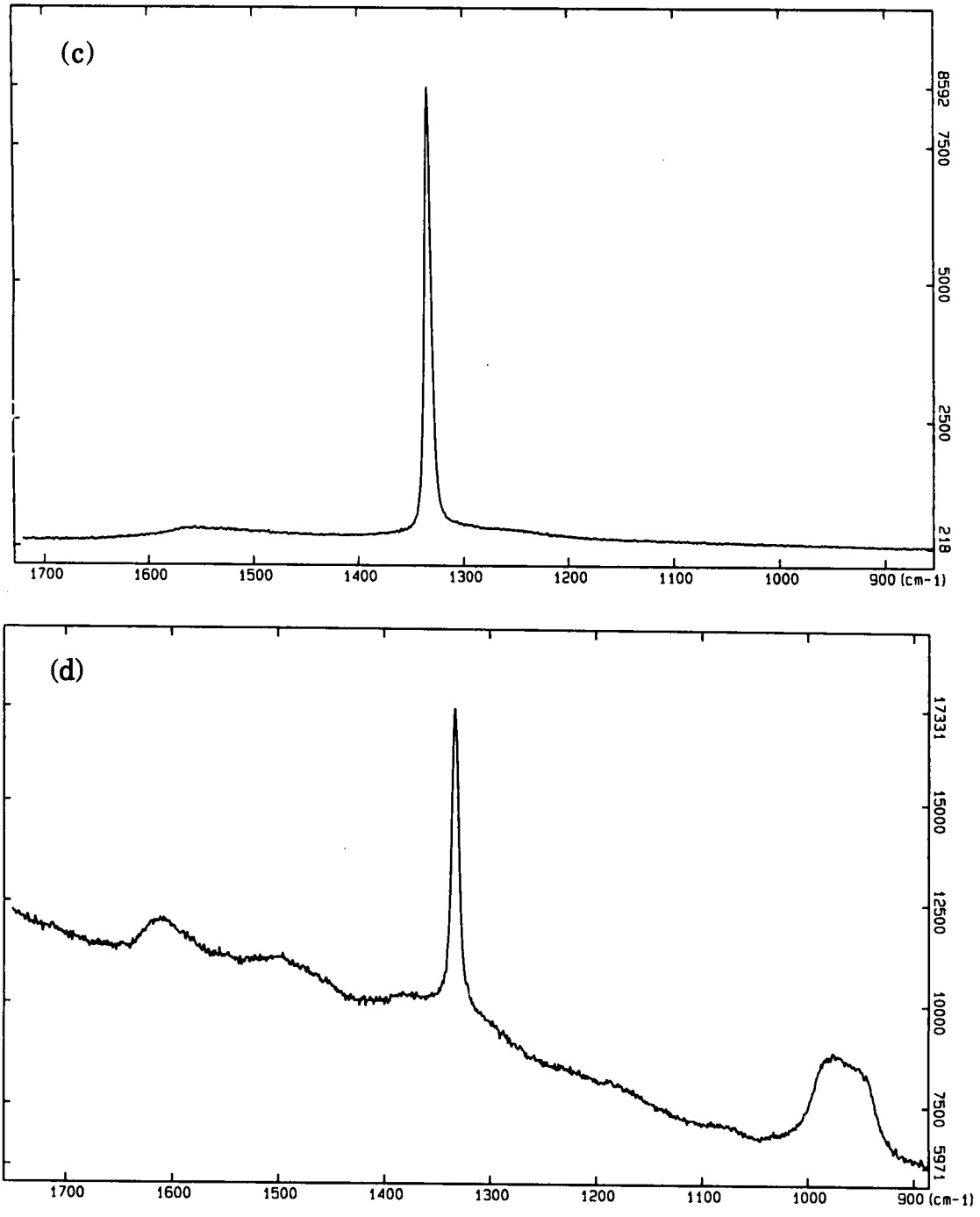


Figure 4.18 (continued) Raman spectra of CVD films. (c) T_f = 2110 °C, T_s = 780 °C; (d) T_f = 1670 °C, T_s = 515 °C.

4.5 Conclusions

The chemistry occurring in a HFCVD reactor during diamond deposition is complex. The current picture of the chemistry involved during CVD diamond film growth consists of the activation or pyrolization of H_2 to H combined with H abstraction and carbon building reactions in the gas phase that interact with the growth surface. Through the use of orifice sampling to probe the near surfaces gases during diamond deposition, insight has been gained on the possible roles of the dominant stable and radical species.

The H REMPI results suggest that the dominant role of H is surface related (e.g. etching or termination of dangling bonds) because the relative H concentration decreased with increasing T_s; and not gas phase related (e.g. preparation of gaseous intermediates) because the relative H concentration did not roll over with increasing T_f. This is supported by the CH_3 REMPI results because CH_3 does not show the same dependence on substrate temperature and this indicates the role of H is surface related. A model presented by Hsu illustrates a similar effect of surface temperature on the gas composition.[65] The H atom destruction probability on the surface was assigned an activation energy (E_a) of 7.3 kcal/mol. This value is similar to the H-atom abstraction value of 6.7 kcal/mol reported by Krasnoperov et al.[66] It was also successfully used to account for the large differences in H-atom destruction probabilities measured at room temperature[67] and 1200 K[68,69] diamond surfaces. The

model predicts that as T_s decreases, the atomic hydrogen mole fraction will increase, thus supporting the results observed (Figure 4.9).

The CH_3 concentration at the surface is determined by filament chemistry, transport in the gas, and surface chemistry. Modeling studies[70,71] have illustrated that away from the substrate, CH_3 concentration is determined by the partial equilibrium of the rapid reaction:

$$CH_4 + H \leftrightarrow CH_3 + H_2 . \qquad (1)$$

If this reaction controls the CH_3 concentration, we have that $[CH_3] \propto [CH_4][H]/[H_2]$ because the equilibrium constant for the reaction is nearly independent of temperature. This reaction could explain the results if it was in partial equilibrium near the substrate and the [H] decreased at low temperatures. However, the partial equilibrium has been shown to break down near the substrate.[33,71]

Another type of gas-phase reaction that may also account for the observed CH_3 results is radical-radical recombination:

$$CH_3 + CH_3 \rightarrow C_2H_6 \qquad (2)$$

or

$$CH_3 + H \rightarrow CH_4 . \qquad (3)$$

Reactions (2) and (3) could be responsible for the observed results because

they are faster at room temperature resulting from their pressure-dependent rate constants with negative temperature exponents.[72]

It is also possible that CH_3 could be produced as a result of H etching of non-diamond carbon on the growth surface. CH_3 is known as a primary etch product of H-attack on amorphous carbon.[73,74] H etching of non-diamond carbon is widely thought to be essential to CVD diamond growth, resulting in the suppression of non-diamond phases. Since H etching has an activation energy of ~ 22.2 ± 8 kJ/mol,[75] if this process occurred rapidly it could produce CH_3 at higher temperatures, leading to a temperature dependence similar to that observed.

The concentration of key radical species, H and CH_3, are not only dependent on the activation controlling parameter, the filament temperature, but are affected by substrate temperature as well. These effects are particularly evident in orifice sampling.

References

References

1. Kiffer, A. D.; Synthesis of diamond from carbon monoxide: Tonawanda Laboratories, Linde Air Products Co., 6 June 1956.

2. Peters, M. G.; Knowles, J. L.; Breen, M.; McGarthy, J. In *Proceedings of the SPIE Conference on Diamond Optics II;* Feldman, A.; Holly, S., Eds.; Electrochemical Society, vol. 1146, 1989.

3. Anthony, T. A. In *Diamond, Boron Nitride, Silicon Carbide and Related Wide Bandgap Semiconductors*; Glass, J.T.; Messier, R.; Fujimori, N., Eds.; Mater. Res. Soc. Proc., vol. 162, Pittsburgh, PA 1990.

4. Yarbrough, W. A.; Messier, R. *Science* 1990, *247*, 688.

5. Wu, C. H.; Tamor, M. A.; Potter, T. J.; Kaiser, E. W. In *Diamond, Boron Nitride, Silicon Carbide and Related Wide Bandgap Semiconductors*; Glass, J.T.; Messier, R.; Fujimori, N., Eds.; Mater. Res. Soc. Proc., vol. 162, Pittsburgh, PA 1990.

6. Koba, R. J. In *Diamond Films and Coatings*; Davis, R.F. Ed; Noyes Publications: New Jersy, 1993, pp 147-182.

7. Matsumoto, S.; Sato, Y.; Tsatsumi, M.; Setaks, N. *J. Mater. Sci.* 1982, *17*, 3106.

8. Matsumoto, S.; Sato, Y.; Kamo, M.; Setaka, N. *Japan. J. Appl. Phys.* 1982, *21*, L183-185.

9. Anthony, T. R. In *Diamond and Diamond-like Films and Coatings*; Clausing, R. E., Ed.; Plenum Press: New York, 1991.

10. Langmuir, I. *J. Amer. Chem. Soc.* 1912, *34*, 860.

11. Langmuir, I. *J. Amer. Chem. Soc.* 1912, *34*, 1310.

12. Singh, B.; Arie, Y.; Lavine, A.; Mesker, R. *Appl. Phys. Lett.* 1988, *52*, 451.

13. Jasen, F.; Chen, I.; Machonkin, A. *J. Appl. Phys.* 1989, *66*, 5749.

14. Stoner, B. R.; Ma, G. H. M.; Wolter, S. D.; Glass, J. T. *Phys. Rev. B* 1992, *45*, 11067.

15. Kawarada, H.; Mar, K. S.; Hiraki, A. *Japan. J. Appl. Phys.* 1987, *26*, L1032.

16. Landstrass, M. I.; Ravi, K. V. *Appl. Phys. Lett.* 1989, *55*, 975.

17. Peters, M. G.; Pinneo, J. M.; Plano, L. S.; Ravi, K. V.; Versteeg, V.; Yokota, S. *SPIE Proceedings* vol 877, 1988.

18. Rudder, R. A.; Posthill, J. B.; Markunas, R. J. *Electronics Letters* 1989, *25*, 1220.

19. Roman, W. C.; Colket, M. B. , In *Diamond and Diamond-like Films*, Dismukes, J. Ed; Electrochemical Society Proceedings, vol. PV 89-12, Pennington, NJ 1989.

20. Matsumoto, S. , In *Diamond and Diamond-like Films*, Dismukes, J. Ed; Electrochemical Society Proceedings, vol. PV 89-12, Pennington, NJ 1989.

21. Hirose, Y.; Kondo, N. , In *Program and Book of Abstracts*, Japan Appl. Phys. Proceedings, 1988.

22. Ravi, K. V.; Koch, C.A.; Hu, H. S; Joshi, A. *J. Mater. Res.* 1990, 5, 2356.

23. Thorsheim, H. R.; Butler, J. E. In *Synthetic Diamond: Emerging CVD Science and Technology*; Spear, K. E., Dismukes, J. P., Eds.; Wiley-Interscience Publication: New York, 1994, pp 193-242.

24. Chapman, B. *Glow Discharge Processes*; Wiley: New York, 1980.

25. Smentkowski, V. S.; Yates, J. T. *J. Vac. Sci. Technol. A* 1993, *11*, 3002.

26. Harris, S.; Weiner, A. M.; Perry, T. A. *Appl. Phys. Lett.* 1988, *53*, 1605.

27. Harris, S. *Appl. Phys. Lett.* 1989, *55*, 2179.

28. Hsu, W. L.; Tung, D. M. *Rev. Sci. Instrum.* 1992, *63*, 4138.

29. Walters, J. D. In *Chemical Instrumentation: A Systematic Approach*; Strobel, H. A., Heineman, W. R., Eds.; Wiley: New York, 1989, pp 896.

30. Green, D. W.; Reedy, G. T. In *Fourier Transform Infrared Spectroscopy*; Farraro, J. R., Basile, L. J., Eds.; Academic: New York, 1978; Vol. 1, pp 1.

31. Andrews, L. *Annu. Rev. Phys. Chem.* 1971, *22*, 109.

32. Chu, C. J.; Bai, B. J.; D'Evelyn, M. P.; Hauge, R. H. , In *Materials Research Society Symposium Proceedings*, vol. 162, 1990.

33. Hsu, W. L. *Appl. Phys. Lett.* 1991, *59*, 1427.

34. Kuritsyn, Y. A. In *Laser Analytical Spectrochemistry*; Letokhov, V. S., Ed.; Adam Hilger: Bristol, UK, 1986, pp 152-228.

35. Celii, F. G.; Pehrsson, P. E.; Wang, H. T.; Nelson, H. H.; Butler, J. E. In *Science and Technology of New Diamond*; Saito, S., Fukunaga, O., Yoshikawa, M., Eds.; Terra Scientific: Tokyo, 1990, pp 17-23.

36. Griffiths, P. R. *Chemical Infrared Fourier Transform Spectroscopy*; Wiley: New York, 1975.

37. Cool, T. A. *Applied Optics* 1984, *23*, 1559.

38. Celii, F. G.; Butler, J. E. , In *Proceedings of the 2nd International Conference on New Diamond Science and Technology*; Mater. Res. Soc., Pittsburg 1991.

39. Butler, J. E.; Celii, F. G. , In *Electrochemical Society Proceedings*; vol. 89(12), 1989.

40. Celii, F. G.; Butler, J. E. *Appl. Phys. Lett.* 1989, *54*, 1031.

41. Celii, F. G.; Pehrsson, P. E.; Butler, J. E., In *Proceedings of the SPIE Conference on Diamond Optics II;* Feldman, A.; Holly, S., Eds.; Electrochemical Society, vol. 1146, 1989.

42. Wiley, W. C.; McLaren, I. H. *Rev. Sci. Instrum.* 1955, *26*, 1150.

43. Opsal, R. B.; Owens, K. G.; Reilly, J. P. *Anal. Chem.* 1985, *57*, 1884.

44. Eltenton, G. C. *J. Chem. Phys.* 1947, *15*, 455.

45. Postek, M. T.; Howard, K. S.; Johnson, A. H.; McMichael, K. L. *Scanning Electron Microscopy -- A Sudent's Handbook*; Ladd Research Industries, Inc., 1980.

46. Plano, L. S.; Adar, F. , In *SPIE Proceedings -- The International Society for Optical Engineering*; San Diego, CA, 1987.

47. Rouzaud, J. N.; Oberlin, O.; Beny-Bassez, C. *Thin Solid Films* 1983, *105*, 75.

48. Wada, N.; Solin, S. A. *Physica* 1981, *105B*, 353.

49. Plano, L. S. *Structure and Chemistry in Diamond-Producing DC Plasmas*: Stanford, CA, 1991.

50. Fite, W. L. ; Expansion of Gases from Molecular Beam Sources, Extranuclear Laboratories, Inc., 1971.

51. Montague, R. G.; Harrison, M. F. A.; Smith, A. C. H. *J. Phys. B: Mol. Phys.* 1984, *17*, 3295.

52. Stephan, K.; Helm, H.; Mark, T. D. *J. Chem. Phys.* 1980, *73*, 3763.

53. Corat, E. J.; Goodwin, E. J. *J. Appl. Phys.* 1993, *74*, 2021.

54. Sommer, M.; Smith, F. W. *J. Mater. Res.* 1990, *5*, 2433.

55. Li, L.; Wu, M.; Johnson, P. M. *J. Chem. Phys.* 1988, *89*, 3470.

56. Moore, C. E. *Atomic Energy Levels*; Government Printing Office: Washington, D.C., 1949.

57. Fedoseev, D. V.; Varnin, V. P.; Deryagin, B. V. *Russian Chem. Rev.* 1984, *53*, 435.

58. Setaka, N. , In *Chemical Vapor Deposition 1987, Proceedings from the 10th International Conference on Chemical Vapor Deposition*; The Electrochemical Society; Pennington, NJ 1987.

59. Saito, Y.; Sato, K.; Tanaka, H.; Fujita, K.; Matsuda, S. *J. Mater. Sci.* 1988, *23*, 842.

60. Hudgens, J. W.; DiGiuseppe, T. G.; Lin, M. C. *J. Chem. Phys.* 1983, *79*, 571.

61. Celii, F. G.; Butler, J. E. *J. Appl. Phys.* 1992, *71*, 2877.

62. Clausing, R. E.; Heatherly, L.; Horton, L. L.; Specht, E. D.; Begun, G. M.; Wang, Z. L. *Diamond Relat. Mater.* 1992, *1*, 411.

63. Wild, C.; Hettes, N.; Koidl, P. *J. Appl. Phys.* 1990, *68*, 973.

64. Wild, C.; Koidl, P.; Müller-Sebert, W.; Walcher, H.; Kohl, R.; Herres, N.; Locher, R.; Samelenski, R.; Brenn, R. *Diamond Relat. Mater.* 1993, *2*, 158.

65. McMaster, M. C.; Hsu, W. L.; Coltrin, M. E.; Dandy, D. S. *J. Appl. Phys.* 1994, *76*, 7567.

66. Krasnoperov, L. N.; Kalinovski, I. J.; Chu, H.-N.; Gutman, D. *J. Phys. Chem.* 1993, *97*, 787.

67. Proudfit, J. A.; Capelli, M. A. In *Proceedings of the 3rd International Symposium on Diamond Materials*; Dismukes, J.P.; Ravi, K.V.; Spear, K.E.; Lux, B.; Setaka, N., Eds.; The Electrochemical Society, vol. 93-17, 1993.

68. Harris, S. J.; Weiner, A. M. In *Proceedings of the 3rd International Symposium on Diamond Materials*; Dismukes, J.P.; Ravi, K.V.; Spear, K.E.; Lux, B.; Setaka, N., Eds.; The Electrochemical Society, vol. 93-17, 1993.

69. Harris, S. J.; Weiner, A. M. *J. Appl. Phys.* 1993, *74*, 1022.

70. Goodwin, D. G.; Gavillet, G. G. *J. Appl. Phys.* 1990, *68*, 6393.

71. Goodwin, D. G.; Gavillet, G. G. In *Proceedings of the International Conference on New Diamond Science and Technology*; Messies, R.; Glass, J.T.; Butler, J.E.; Roy, R., Eds.; Materials Research Society, 1991.

72. Warnatz, J. In *Combustion Chemistry*; Gardiner, W. C., Ed.; Springer: New York, 1984, pp 197.

73. Vietzke, E.; Flaskamp, K.; Philipps, V.; Esser, G.; Wienhold, P.; Winter, J. *J. Nucl. Mater.* 1987, *145-147*, 443.

74. Hsu, W. L. *J. Vac. Sci. Technol. A* 1988, *6*, 1803.

75. Rye, R. R. *Surf. Sci.* 1977, *69*, 653.

Appendix

Appendix

1. Number of ions per pulse calculation:

100 sccm into chamber

↓

25 sccm through orifice

↓

0.4 scc/sec

↓ (2×10^{19} particles/cc @ STP)

1×10^{19} particles/sec

↓ (6×10^{-4} intercept)

6×10^{15} partilces/sec through skimmer

↓ (5% Ne)

3×10^{14} particles/sec (Ne)

↓ (μs)

2.1×10^{9} particles

↓

$$(1-\frac{I_T}{I_0}) = 1 - e^{-N\sigma x}$$

$$= 1-e^{-(2.1\times10^{9})(0.5\times10^{-16})(1)}$$

$$= 1.05\times10^{-7}$$

EM Current = 0.5 mA (90% of flux)

↓ (10% flat passes slit)

55 μA

↓ (10^{19} e-/sec)

5.5×10^{14} e-/sec

↓ (7μs)

3.85×10^{9} e-

↓ 1.05×10^{-7}

404 ions

2. Type of flow calculation:

$$PV = nRT$$

$$\frac{N}{V} = \frac{P}{kT}$$

$$= \frac{(80\ \text{Torr})(6.022\text{x}10^{23}\text{mol}^{-1})}{(62.364\ \frac{\text{L Torr}}{\text{K mol}})(1000\ \text{K})} \text{ x } \frac{1}{1000\ \text{cm}^3}$$

$$= 7.7\text{x}10^{17}\ \text{cm}^{-3}$$

$$D \cdot n_s = 7.7\text{x}10^{17}\ \text{cm}^{-3} \cdot 2.0\text{x}10^{-2}\ \text{cm}$$
$$= 1.5\text{x}10^{16}\ \text{cm}^{-2}$$

Compares to Fite's condition for flow:

$D \cdot n_s << 10^{14}$ to 10^{15} cm^{-2} for Effusive Flow

3. Conductance calculations:

Laminar flow: $d\bar{p} > 6\text{x}10^{-1}$ mbar · cm
Molecular flow: $d\bar{p} < 10^{-2}$ mbar · cm

From growth region to expansion region:

$$(200\text{x}10^{-4}\text{cm})(\frac{110 + 1\text{x}10^{-3}}{2}) = 1.1\ \text{mbar} \cdot \text{cm}\ \ \textbf{(Laminar)}$$

From expansion region to mass spectrometer:

$$(0.05\ \text{cm})(\frac{1\text{x}10^{-3} + 4\text{x}10^{-6}}{2}) = 2.5\text{x}10^{-5}\ \text{mbar} \cdot \text{cm}\ \textbf{(Molecular)}$$

Conductance for Laminar Flow (growth region to expansion region):

$$C = 76.6\,\delta^{0.712}(1 - \delta^{0.258})^{0.5} \text{ x } \frac{A}{1 - \delta} \qquad \text{A is in cm}^2$$

$$\delta = \frac{p_2}{p_1} = 1.25\text{x}10^{-5}$$

$$C = (76.6)(3.23\text{x}10^{-4})(0.973)(3.14\text{x}10^{-4})$$
$$= 7.6\text{x}10^{-6}\ \text{liters/sec Air x 2.07 (correction for } H_2)$$
$$= 1.6\text{x}10^{-5}\ \text{liters/sec}$$

Pressure determination for Laminar Flow:

$pS = C\,(p_1 - p_2)$
$p\ (250\ \text{liters/sec}) = (1.6\text{x}10^{-5})(110\ \text{mbar} - 1\text{x}10^{-3}\ \text{mbar})$
$p = 5\text{x}10^{-6}\ \text{Torr}$

Conductance for Molecular Flow (expansion region to mass spectrometer):

$C = 11.6\ A$
$= (11.6)(\pi(\frac{0.05}{2})^2)$
$= 2.3\text{x}10^{-2}$ liters/sec Air x 3.77 (correction for H_2)
$= 8.6\text{x}10^{-2}$ liters/sec

Pressure determination for Molecular Flow:

$pS = C\,(p_1 - p_2)$
$p\ (1060\ \text{liters/sec}) = (8.6\text{x}10^{-2}\ \text{liters/sec})(1\text{x}10^{-3}\ \text{mbar} - 4\text{x}10^{-6}\ \text{mbar})$
$p = 6\text{x}10^{-8}\ \text{Torr}$

Vita

Lenora Lorraine Jones (Lenni) was born in Iron Mountain, Michigan on December 30, 1969. She moved often during childhood living in such locals as: Wisconsin, El Salvador, Connecticut, and Virginia. Upon graduation from Hermitage High School in June of 1988, she entered Saint Andrews Presbyterian College in Laurinburg, North Carolina where she went on to become President of the Student Government Association and a member of Who's Who Among Students in American Universities and Colleges. She received a Bachelor of Science in chemistry and a Bachelor of Arts in mathematics, in May of 1992. In August of 1992, she began her graduate studies at the University of Tennessee, Knoxville and successfully completed the requirements for a Master of Science degree in August of 1995.